



PII S0016-7037(00)00379-3

## Geologic control of Sr and major element chemistry in Himalayan Rivers, Nepal

N. B. ENGLISH,\* J. QUADE, P. G. DECELLES, and C. N. GARZIONE  
Department of Geology, University of Arizona, Tucson, AZ 85721, USA

(Received June 7, 1999; accepted in revised form February 29, 2000)

**Abstract**—Our study of the Seti River in far western Nepal shows that the solute chemistry of the river and its tributaries is strongly controlled by geology. The Seti flows through four distinct terranes, starting with the Tethyan sedimentary series (TSS) and Greater Himalayan series (GHS). TSS/GHS waters display  $^{87}\text{Sr}/^{86}\text{Sr}$  ratios of  $<0.73$  and high Sr and Ca, consistent with the composition of limestone and marble common in these terranes. The  $^{87}\text{Sr}/^{86}\text{Sr}$  ratio and Mg increase markedly as the river passes into the Lesser Himalayan series (LHS), where tributaries have  $^{87}\text{Sr}/^{86}\text{Sr}$  ratios from 0.75 to 1.02 and high Sr, Ca, and Mg. The high Mg in LHS waters correlate with high  $^{87}\text{Sr}/^{86}\text{Sr}$  ratios, which we attribute to weathering of highly radiogenic (0.71–0.82) dolostones. Tributaries to the Seti River draining the largely carbonate-free Dadeldhura thrust sheet (DTS) have ratios near 0.74, but low Sr, Ca, and Mg and therefore have little impact on Seti mainstem chemistry. Mass balance calculations and CaMg-weathering indices show that carbonate weathering accounts for  $>70\%$  of total dissolved solids to the Seti River. Sr/Ca ratios of river waters provide a minimum estimate of the %-carbonate weathering contribution to Sr, due to partitioning of Sr and Ca during incongruent dissolution and reprecipitation of calcite. Overall, we attribute high  $^{87}\text{Sr}/^{86}\text{Sr}$  ratios in the Seti River and its tributaries to the weathering of metacarbonates (especially dolostones in the upper Nawakhot Group) which have exchanged Sr with silicates during metamorphism. Our modeling of Sr fluxes in the Seti River indicates that the TSS/GHS accounts for 36–39% of the Sr, the LHS for 40–53%, and 8–23% for the DTS. Prior to exposure of LHS rocks at  $\sim 12$  Ma, TSS and GHS carbonates with low  $^{87}\text{Sr}/^{86}\text{Sr}$  ratios dominated Himalayan rivers. We attribute the elevated  $^{87}\text{Sr}/^{86}\text{Sr}$  ratios of Himalayan paleorivers during the late Miocene and Pliocene to exposure and weathering of LHS metacarbonates. Copyright © 2000 Elsevier Science Ltd

### 1. INTRODUCTION

Indo-Asian collision beginning at 50 Ma produced today's largest mountain range, the Himalaya. The volume of material eroded from the Himalaya and deposited in the Bengal Fan makes the Himalayan orogeny, and the rivers that drain it, central to resolving the relationship between silicate weathering and reductions in atmospheric  $\text{CO}_2$  in the Cenozoic (Raymo and Ruddiman, 1988; Molnar et al., 1993). The modern Ganges–Brahmaputra river system provides 24% of the global sediment flux and  $\sim 9\%$  of dissolved solids to the world's oceans (Berner and Berner, 1987; Raymo and Ruddiman, 1992). Coincident with Himalayan uplift and the development of the Ganges–Brahmaputra river system is a dramatic increase in marine  $^{87}\text{Sr}/^{86}\text{Sr}$  ratios, from 0.7078 in the late Eocene to 0.7091 at present (DePaolo and Ingram, 1985). Some workers (Singh et al., 1998; Edmond, 1992; Raymo and Ruddiman, 1992; Krishnaswami et al., 1992) have attributed the Cenozoic rise in marine  $^{87}\text{Sr}/^{86}\text{Sr}$  ratios and the concurrent fall in atmospheric  $\text{CO}_2$  to the weathering of silicate rocks in the Himalaya. In contrast, other workers (Pearson and Palmer, 1999) find atmospheric  $\text{CO}_2$  in the middle Eocene was similar to modern-day levels with no dramatic draw down related to Himalayan uplift. Over long time scales ( $10^6$  yr), weathering of silicates draws down atmospheric  $\text{CO}_2$  by sequestering 1 mol of  $\text{CO}_2$  in marine carbonates for every 2 mol of  $\text{CO}_2$  consumed from the atmosphere. In contrast,

there is no net, long-term consumption of atmospheric  $\text{CO}_2$  when carbonates are weathered.

Most authors agree that carbonate weathering dominates the major ionic budget of Himalayan rivers, with values ranging from  $>60\%$  (Singh et al., 1998) to  $>90\%$  (Blum et al., 1998). However, there is still considerable disagreement over the proportions of Sr derived from silicate and carbonate weathering. Several recent papers suggest that carbonate weathering dominates Sr fluxes in some Himalayan rivers, including vein carbonate and metasedimentary carbonate in the Greater Himalayan series (GHS) crystalline rocks (Blum et al., 1998), sedimentary carbonate in the Tethyan sedimentary series (TSS); and metasedimentary carbonate in the Lesser Himalayan series (LHS; Palmer and Edmond, 1992; Quade et al., 1997; Harris et al., 1998). In contrast, Sr budgets calculated using Sr/Ca ratios of bedrock and water attribute  $>60\%$  (Singh et al., 1998) and  $>40\text{--}50\%$  of Sr to silicate weathering (Galy et al., 1999), with the remainder divided between carbonates and evaporites.

This paper further examines the sources of Himalayan Sr by combining geologic observations with detailed geochemical measurements of the Seti River watershed as the Seti passes through all four major Himalayan terranes. We find that the solute chemistry of the Seti River and its tributaries is strongly controlled by bedrock. This data set allows us to assign Sr fluxes and  $^{87}\text{Sr}/^{86}\text{Sr}$  ratios to each major terrane. From these results we can calculate the impact that changes in the exposure of major Himalayan terranes through time, reconstructed from petrographic and structural evidence (DeCelles et al., 1998a,b), has on the  $^{87}\text{Sr}/^{86}\text{Sr}$  ratio of ancestral Himalayan rivers.

\* Author to whom correspondence should be addressed (nenglish@geo.arizona.edu).

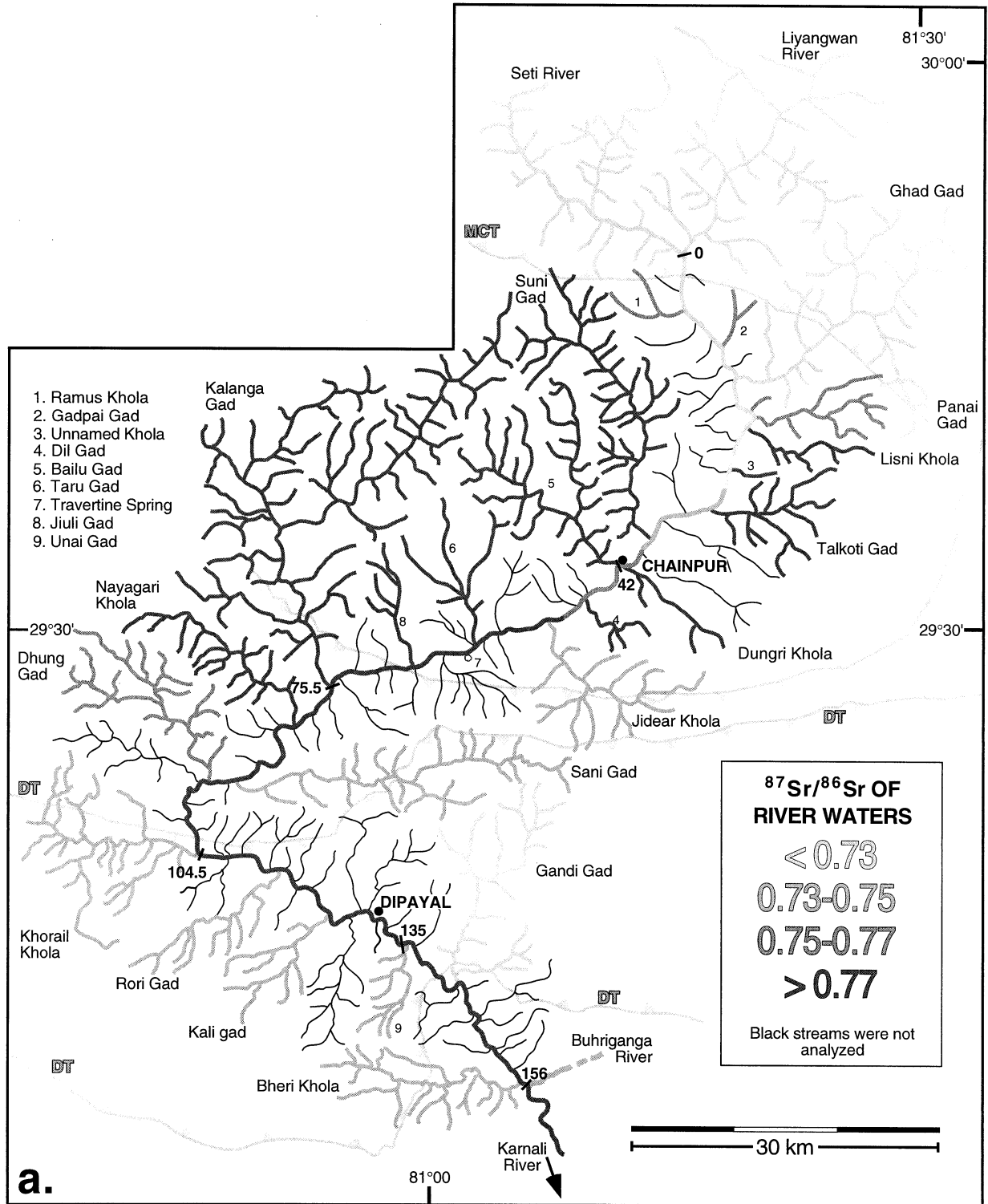


Fig. 1. Map of the Seti River watershed and geology: (a) Gray scale denotes  $^{87}\text{Sr}/^{86}\text{Sr}$  ratios of filtered river water (Table 3), lighter gray denotes lower  $^{87}\text{Sr}/^{86}\text{Sr}$  ratios. In general, rivers with relatively low ratios drain TSS/GHS rocks and rivers with high ratios drain LHS rocks. The Buhriganga River drains the area to the east of the Seti River, but is not shown entirely. Chairu Khola drains the area south of Bheri Khola and is not shown. Bold numbers denote channel distance (km) downstream from the Seti–Liyangwan confluence. The Seti River joins the Karnali River at kilometer 180. Major towns are in bold type. Rivers were sampled at tributary confluences. (b) Regional map with Seti River in small box. (c) Geology is modified from DeCelles et al. (1998a) and general in nature. Rivers are for reference only. STD = South Tibetan detachment fault; MCT = Main Central thrust; DT = Dadeldhura thrust; RT = Ramgarh thrust.



## 2. GEOLOGIC SETTING

### 2.1. Geologic Units and Structure

Careful consideration of geology is essential to assessing the link between river and local bedrock geochemistry. The Seti River drains four lithostratigraphically and structurally distinct zones from north to south (Fig. 1): the Tibetan Himalaya, the Greater Himalaya, and metasediments and crystalline rocks of the Lesser Himalaya. The Seti is tributary to the Karnali River, which drains a final zone, the Subhimalaya.

In the highest watersheds, the Seti River flows through ~23 km of the TSS. The TSS underlies most of the northern half of the Himalayan fold-thrust belt and covers the Tibetan Himalayan zone in our study area. The TSS consists of low-grade metasedimentary and sedimentary rocks of Cambrian to Eocene age, mostly limestone and fine-grained siliciclastic rocks (Burg and Chen, 1984; Searle, 1986).

The Greater Himalayan zone is structurally overlain by the TSS and exposed for ~15 km along the Seti River. It is underlain by the GHS. The GHS is an ~5- to 20-km-thick package of mainly Late Proterozoic amphibolite-grade schists, gneisses, and calc-silicates and is intruded by Paleozoic granites. Carbonate-rich phyllite, marble, and felsic gneiss are present in and below the Main Central thrust.

The Lesser Himalayan zone rests below the Main Central thrust (MCT) and is exposed through ~180 km of the Seti River traverse. The Lesser Himalayan zone is comprised of metasediments of the LHS and of crystalline and metasedimentary rocks of the Dadeldhura thrust sheet (DTS). Thrust repetition of the section exposes the LHS over a large area. The Lesser Himalayan series is a thick succession of mainly quartzite, phyllite, and carbonate divided into the lower and upper Nawakhot Groups.

The lower Nawakhot Group of the LHS is dominated by Early Proterozoic quartzite and phyllite divided into several formations. The Kushma Formation is the basal quartzite of the observable LHS. Overlying the Kushma, the Ranimata Formation is a gritty, chloritic phyllite locally intruded by hornblende diorite and large concordant sills of granitic augen gneiss, referred to as the Ulleri Gneiss. The Sangram, Galyang, and Syanga Formations compose the upper lower Nawakhot and lower upper Nawakhot Group and represent a small proportion of outcrop in the Seti River watershed. The Lakharpata Formation, mainly stromatolitic dolostone and limestone, forms the uppermost upper Nawakhot Group. It is widely exposed in the LHS and abundant in Seti River gravels. Lakharpata Formation rocks are separated into an upper and lower unit by the Benighat Slate. The sandstone, siltstone, and limestones of the Amile, Bhainskati, and Dumri Formations (lower Cretaceous to lower Miocene) rest unconformably on the Lakharpata Formation and are only locally exposed in the study area.

The DTS is a crystalline nappe structurally overlying the LHS along the Dadeldhura thrust (DT). The DTS is exposed for 40 km along the Seti River downstream of the LHS. The DTS is composed of gneiss, coarse mica schist, and phyllite overlain by greenschist-grade phyllite, slate, and quartzite of the Phulchauki Group. The pegmatitic Dadeldhura Granite is a coarse to fine-grained pegmatitic granite intruding the Phulchauki Group. The Kalikot Schist, the Buhri Gandaki (Cambrian–Ordovician)

and Salyani Gad Gneisses are also present in the DTS (DeCelles et al., in press). Another exposure of LHS downstream of the DTS separates the DTS from the Siwalik Group.

The Siwalik Group underlies the LHS beneath the Main Boundary thrust (MBT). The Seti River joins the Karnali River above the MBT and so does not drain Siwalik Group rocks. The Siwalik Group consists of foreland basin sediments deposited by rivers draining the ancestral Himalaya. It rests unconformably above the Eocene Bhainskati formation.

Our understanding of the exposure history of each terrane in the fold-thrust belt, and the basis of our Sr flux model later in this paper, is based on thermochronology data, cross-cutting and overlapping relations and from Siwalik Group provenance data (DeCelles et al., 1998a,b). Initial thrusting began to expose Tethyan sediments between Eocene and Oligocene time. Later thrusting in the Early Miocene along the MCT exposed the GHS (Macfarlane, 1993; Hodges et al., 1996). Repeated thrusting and duplex development within the LHS began in the Middle Miocene (~12 Ma) and widely exposed the LHS by ~5 Ma.

### 2.2. Hydrologic Data

The Seti River watershed drains a 5336-km<sup>2</sup> watershed (5045 km<sup>2</sup> above the confluence of the Buhriganga River) and is tributary to the Karnali, Ghaghara, and ultimately the Ganges River. From its origin at >5000 masl, the Seti River falls through approximately 4700 m of elevation over its ~210 km length. Sampled watersheds range in size from 6 km<sup>2</sup> to >600 km<sup>2</sup> and often drain more than one rock formation or group. The Buhriganga River, a large tributary that flows through multiple terranes, joins the Seti River at kilometer 156.25 (Fig. 1). The Karnali River, which the Seti River joins below the Buhriganga, drains a higher proportion of the TSS than the Seti River and also drains the Siwalik Group in its lower reaches.

Most land adjacent the Seti River remains in a natural state, although small pockets of agricultural terraces along the river are common between Chainpur and Dipayal. No manufactured fertilizers are used on the terraces and the watershed is roadless except between Khorail Khola and Dipayal (kilometer 104.5 and ~130, Fig. 1). Thus, the Seti River and its tributaries provide a largely undisturbed, 156-km-long natural laboratory for evaluating bedrock influences on weathering and Sr budgets.

### 2.3. Meteorologic Data

In general, rainfall amounts increase with elevation. Pokhara, at ~1200 m and 300 km east–southeast of Chainpur, receives an average of  $4.2 \pm 0.4$  m/yr of precipitation (Central Bureau of Statistics, 1998; Fig. 1). Nepalganj, on the Gangetic Plains, receives  $1.3 \pm 0.3$  m/yr. Dipayal, at 580 masl within the Seti River watershed, receives  $1.1 \pm 0.2$  m/yr. The period of record is from 1993 to 1996 and errors are one sigma. The precipitation profile used for modeling is from Masek et al. (1994) and is based on data from the World Health Organization.

## 3. METHODS

### 3.1. Field Collection

Seti River and tributary waters, bedrock, river pebbles, sand and silt samples were collected during a single 30-day foot traverse of the Seti River in April 1997. Mainstem samples were taken above tributary

Table 1. Effects of sample processing on carbonate detritus  $^{87}\text{Sr}/^{86}\text{Sr}$  and Ca/Mg ratios.

Sample location	Uncrushed		Crushed		Uncrushed with ammonium acetate wash		Crushed with ammonium acetate wash		$^{87}\text{Sr}/^{86}\text{Sr}$ of waters
	$^{87}\text{Sr}/^{86}\text{Sr}$	Mg/Ca <sup>a</sup>	$^{87}\text{Sr}/^{86}\text{Sr}$	Mg/Ca	$^{87}\text{Sr}/^{86}\text{Sr}$	Mg/Ca	$^{87}\text{Sr}/^{86}\text{Sr}$	Mg/Ca	
Liyangwan River	0.716902	0.07	0.717717	—	—	—	0.717433	—	0.717673
Seti above Ramus Khola	0.717617	0.08	0.717320	—	—	—	0.717049	—	0.721803
Seti above Talkoti Gad	0.716106	0.09	0.718544	0.12	—	—	—	—	0.736024
Seti below Panai Gad	0.716944	0.06	0.719313	0.13	—	—	—	—	0.726655
Seti above Suni Gad	0.717821	0.10	—	—	0.717441	0.07	—	—	0.736748
Dungri Khola	0.812258	0.82	—	—	0.855743	1.02	0.862562	0.99	0.950671
Bailu Gad	0.872169	0.89	—	—	0.773043	1.06	1.012254	0.94	1.022884
Dil Gad	0.738230	0.90	—	—	—	—	0.748378	0.93	0.798606
Seti above Jidear Khola	0.718327	0.15	—	—	—	—	0.721527	0.13	0.783622
Seti above Jiuli Khola	0.738821	0.45	0.732589	0.35	0.720200	0.42	0.727908	0.38	0.785418
Jiuli Gad	0.727245	0.84	0.772087	—	—	—	0.771832	—	0.783687
Kalanga Gad	0.746054	0.77	0.765521	0.77	—	—	0.766705	—	0.802487
Seti above Nayagari Khola	0.738354	0.82	0.738719	—	—	—	0.744074	0.57	0.779755
Nayagari Khola	0.762711	0.59	—	—	—	—	0.750769	—	0.783503

<sup>a</sup> mol/mol.

confluences and at least one large bend downriver of confluences to allow mixing of waters. Water samples were passed through a disposable 0.2  $\mu\text{m}$  glass syringe filter and collected in acid-washed polyethylene bottles. Distilled water spiked with low concentrations of NBS-987 and similarly filtered yielded a ratio of  $0.710241 \pm 30$ , within error of the standard (NBS-987 =  $0.710250 \pm 10$ ; all  $^{87}\text{Sr}/^{86}\text{Sr}$  ratio errors are  $2\sigma$ ). Water and sediment samples were kept dark during field transport and refrigerated during storage.

Sand and silt-size fractions of sediment were collected from water sample sites. Only sediments from above confluences (tributary and Seti River) were analyzed, as these probably represent the most homogeneous sediments from the Seti River and its tributaries. Still, sediments from tributaries and the Seti River may only represent sediment from one depositional event or a disproportionate sediment mixture from several watersheds upstream of the confluence. Carbonate pebbles and rocks were collected from river sediments, bedrock exposures, and several large (>10 m) colluvial boulders (phyllitic marbles only). Representative bedrock samples were collected from each terrane. Boulder counts from gravel bars along the Seti River include all the cobbles and large pebbles from an approximately 1 m<sup>2</sup> area near water and sediment sample locations.

River waters were filtered and titrated in the field immediately after collection using 0.005M HCl and a HANNA<sup>TM</sup> HC-9055 electronic pH meter with temperature probe and calibration. Three titrations from the same water collected multiple times within the same hour yielded total alkalinities within 3% of each other. Results from field titrations were later used to evaluate the accuracy of major cation data and for mass balance calculations.

### 3.2. Sample Preparation

Carbonate rocks were crushed and soaked in doubly distilled 1M acetic acid, put in an ultrasonic bath for 30 min and let stand 14 h at 20°C. Silicate rocks were digested in hot HF-HNO<sub>3</sub> overnight. After dissolution, carbonate and silicate digests were centrifuged, decanted and rinsed with 18 M $\Omega$  H<sub>2</sub>O three times. The supernatant was then evaporated to dryness and dissolved in 2.5 M HCl.

Most sediment samples were left uncrushed prior to pretreatment. Sediments were washed in 3% H<sub>2</sub>O<sub>2</sub> to eliminate the Sr from modern organic detritus, rinsed four times in 18 M $\Omega$  H<sub>2</sub>O and then treated with doubly distilled acetic acid to dissolve the carbonate fraction, in the same way as carbonate rocks. Some sediment subsamples were crushed and then washed in 0.2M ammonium acetate (after Montañez et al., 1996) to evaluate the potential impact of crushing sediments and of leaching silicate minerals in acetic acid.

### 3.3. Sample Analysis

Percent carbonate ( $\pm 3\%$ ) of sand and silts was determined by weight loss upon dissolution of approximately 1 g of sand in 10% HCl for 12 h. The error is produced by the loss of clays in suspension while decanting the sample. Samples sat overnight and were then decanted, rinsed, and centrifuged twice. Percent limestone and dolostone in pebbles and bedrock were determined using molar concentrations of acetic acid leaches.

Major cation and anion concentrations for waters were determined to within  $\pm 10\%$  by inductively coupled plasma and ion chromatography, respectively. Repeat analyses were performed on samples that did not charge balance to within 12% of measured total alkalinity. Mineral saturation indices (log IAP/KT) were determined using WATEQ4F. Carbonate rock and sediment digests were analyzed for Ca, Mg, and Sr using ion chromatography. All Sr/Ca ratios are expressed as nmol/ $\mu\text{mol}$  and Mg/Ca ratios as mol/mol. Strontium from waters, sediment, and rock digests was separated with ion-specific resin and  $^{87}\text{Sr}/^{86}\text{Sr}$  ratios were measured on a Micromass Sector 54 thermal ionization mass spectrometer to a precision of at least  $\pm 71$  ( $2\sigma$ ). The  $^{88}\text{Sr}/^{86}\text{Sr}$  ratio was normalized to 0.1194 and analyses of the NBS-987 standard run on each 20-sample turret yielded a mean ratio of  $0.710262 \pm 12$  ( $1\sigma$ ,  $n = 62$ ).

### 3.4. Effects of Sediment Crushing and Ammonium Acetate Pretreatment

Crushing variously affects Sr results from detrital carbonate. Crushed and uncrushed TSS/GHS sediment yield similar  $^{87}\text{Sr}/^{86}\text{Sr}$  ratios. However, crushed sediment from LHS tributaries yields higher  $^{87}\text{Sr}/^{86}\text{Sr}$  ratios than uncrushed subsamples (Table 1). In the LHS samples, carbonate was still present in our detrital samples even after 14 h in 1 M acetic acid. We conclude that the difference between crushed and uncrushed is caused by greater dissolution of  $^{87}\text{Sr}$ -rich dolostones in crushed sediments.  $^{87}\text{Sr}/^{86}\text{Sr}$  ratios of acetic acid leaches from uncrushed LHS carbonate therefore underestimate bulk carbonate detritus  $^{87}\text{Sr}/^{86}\text{Sr}$  ratios.

Appreciable quantities of silicate minerals are present in our carbonate rock samples and stream detritus samples. Dissolution of carbonate/silicate mixtures with weak acetic acid has been shown not to significantly leach Sr from silicates (Asahara et al., 1995; Quade et al., 1995). However, some Himalayan silicates, particularly in the LHS, are highly radiogenic ( $^{87}\text{Sr}/^{86}\text{Sr} > 1.0$ ). Our concern is that minor leaching of Sr from LHS silicates during the acetic acid dissolution would contaminate the supernatant. Pretreatment with ammonium acetate has been

shown to very effectively minimize this effect in other studies, by removal of Sr from exchange sites on silicates (Montañez et al., 1996). We found that pretreatment with ammonium acetate had no effect on some results while mostly lowering the  $^{87}\text{Sr}/^{86}\text{Sr}$  ratio in others, but in nearly all cases not appreciably ( $n = 14$ ;  $|\text{mean difference}| = 0.0082$  excluding Dungri Khola). Elevated  $^{87}\text{Sr}/^{86}\text{Sr}$  ratios in Dungri Khola sediments treated with ammonium acetate may be the result of heterogeneous subsamples or of relatively low  $^{87}\text{Sr}/^{86}\text{Sr}$  strontium being washed from exchangeable sites. Other studies (Singh et al., 1998) using the same acetic acid treatments on similar rocks did not observe substantial leaching of Rb, again an indication that the silicates are not being leached. We are continuing to experiment with our dissolution procedures.

#### 4. RESULTS AND DISCUSSION

Our results have important implications for three broad issues, around which we will organize our presentation of results and discussion: first is the influence that bedrock and sediment has on total dissolved solids (TDS) and Sr in Himalayan rivers; second, is the relative weathering contributions to river TDS from silicate and carbonate rocks in small and large watersheds within the Seti River watershed; third, is the relative contribution of silicate and carbonate weathering to the Sr budget of the Seti River. This discussion includes a critical evaluation of Sr/Ca ratios and their use in distinguishing Sr derived from silicate versus carbonate weathering. Finally, we speculate on the impact of Himalayan tectonic evolution on the riverine Sr budget of the Ganges–Brahmaputra River system over the past 25 Ma.

##### 4.1. Bedrock and Sediment Control of Riverine TDS and Sr

The Seti and tributary rivers display dramatic downstream changes in major element and  $^{87}\text{Sr}/^{86}\text{Sr}$  chemistry (Fig. 2), changes that coincide with the major terrane boundaries (Figs. 1, 3). The Seti mainstem and large tributaries traverse  $>23$  km of TSS. The highest water samples taken in our traverse, at the Seti–Liyangwan confluence, come from within the GHS zone,  $\sim 3$  km downstream from the last outcrops of the TSS. Limestone, phyllite, and quartzite in the river bedload at this point are derived largely from the TSS. TSS limestone far outnumber dolomite and marble in the clast counts (Fig. 4).  $^{87}\text{Sr}/^{86}\text{Sr}$  ratios of the carbonate detritus (range 0.7167–0.7169) and fluvial limestone clasts are among the lowest of any carbonates sampled on this traverse ( $n = 9$ ; mean 0.7227; range 0.7113–0.7520). They are closely matched by low  $^{87}\text{Sr}/^{86}\text{Sr}$  ratios (0.7178–0.7194) of associated river water (Tables 2 and 3). River water is high in TDS ( $>87$  mg/L), in Sr (890–1746 nmol/L), and has high  $(\text{Ca} + \text{Mg})/(\text{Na} + \text{K} + \text{Si})$  (Fig. 3).

Downstream, the Seti mainstem passes through an  $\sim 15$  km zone of GHS and MCT rocks, which is reflected by an increase in high-grade metamorphic silicate and marble clasts in bedload counts. Sampled tributaries draining largely GHS/MCT-zone rocks include Gadpai, Ramus, and Ghad Gad, while Panai Gad also drains LHS rocks. Percent carbonate in mainstem sands drops slightly to 18%, reflecting lower %-carbonate (7–12%) in local tributaries along this reach (Table 2). The only type of carbonate clast found in these tributaries is marble schist, except in Panai Gad, where clasts of pink dolostone (probably LHS derived) dominate.  $^{87}\text{Sr}/^{86}\text{Sr}$  ratios of calcite in marble clasts average 0.7156 ( $n = 11$ ; range 0.7111–0.7240),

whereas sand-size carbonate detritus ranges from 0.7151 to 0.7957. The sands with high ratios (Panai and Gadpai Kholas) also have high Mg/Ca, suggesting these tributaries are carrying some dolostone from the LHS. The high  $^{87}\text{Sr}/^{86}\text{Sr}$  ratios (between 0.7283 and 0.7651) of the tributary waters mimic elevated ratios of detrital carbonate. Carbonate in the sand fraction of the Seti mainstem retains the low  $^{87}\text{Sr}/^{86}\text{Sr}$  ratios (0.716) of the TSS, and thus appears little impacted by additions from tributaries with radiogenic carbonates.  $^{87}\text{Sr}/^{86}\text{Sr}$  ratios of mainstem waters rise modestly from 0.7203 to 0.7267, in response to discharge from local tributaries.

Below the MCT, the Seti begins its traverse through the LHS. The first 20 km of this reach (down to Suni Gad) cuts through rocks of the lower Nawakhot Group, composed of quartzite and phyllite but little or no carbonate. Unnamed Khola and Talkoti Gad carry no sand-size detrital carbonate, whereas Lisni Khola carries 17%. Tributaries draining these rocks have low TDS, low Sr, and high  $^{87}\text{Sr}/^{86}\text{Sr}$  ratios. Their contribution dilutes mainstem TDS and Sr but increases  $^{87}\text{Sr}/^{86}\text{Sr}$  ratios of mainstem waters from 0.7267 to 0.7367.

$^{87}\text{Sr}/^{86}\text{Sr}$  ratios of mainstem waters increase sharply as the Seti next passes into  $\sim 80$  km of thrust-imbricated rocks of the upper and lower Nawakhot Group. This increase begins just below the confluence with Suni Gad, the first tributary to carry abundant, highly radiogenic dolostones of the upper Nawakhot Group (Figs. 1, 2). Throughout the LHS, dolostone dominates limestone in clast counts (Fig. 4), and has average  $^{87}\text{Sr}/^{86}\text{Sr}$  ratios of 0.7509 ( $n = 11$ ; range 0.7110–0.8208). The addition of Lesser Himalayan dolostone to mainstem bedload is reflected in clast counts and increases in Mg/Ca from 0.10 to 0.82 in sand-size carbonate detritus. Percent detrital carbonate ranges from 6 to 25%.  $^{87}\text{Sr}/^{86}\text{Sr}$  ratios of carbonate detritus in tributaries average 0.7782 ( $n = 10$ ; range 0.7215–1.01). Ratios of carbonate detritus in the mainstem generally increase downstream and vary between 0.7215 and 0.7441. The large increase in  $^{87}\text{Sr}/^{86}\text{Sr}$  ratios of carbonate detritus due to dolostone addition coincides with the largest increases anywhere in the traverse in mainstem TDS, total  $\text{Mg}^{2+}$ , Mg/Ca, and  $^{87}\text{Sr}/^{86}\text{Sr}$  ratios (Figs. 2, 5, 6).

Below the LHS, the Seti River traverses the DTS for  $\sim 40$  km. The DTS is dominated by gneisses, quartzite, and schist. DTS tributaries include Khorail Khola, Kali Gad, Unai Gad, Rori Gad, Bheri Khola and Gandi Gad. Carbonate is not present in the bedload of any DTS tributary except Gandi Gad. However, dolostone and some limestone clasts persist in the mainstem, derived from the TSS and LHS upstream. All tributaries except Gandi Gad display very low TDS, low Sr, and average 0.7344 (range 0.7274–0.7379) in  $^{87}\text{Sr}/^{86}\text{Sr}$  ratios. Low  $(\text{Ca} + \text{Mg})/(\text{Na} + \text{K} + \text{Si})$  in the DTS tributaries distinguish them from local Seti mainstem values and tributaries upstream draining carbonate rocks (Fig. 3). The addition of DTS tributary water has virtually no effect on TDS, Sr, or  $^{87}\text{Sr}/^{86}\text{Sr}$  ratios of mainstem waters. The low total dissolved solids of DTS tributary waters is characteristic of silicate weathering and explains the negligible impact of DTS rock weathering on Seti mainstem chemistry (Figs. 2, 3).

Below the DTS, the Seti reenters the LHS before joining the Buhriganga River  $\sim 14$  km downstream. Along this 14 km reach, LHS is composed entirely of quartzite (Kushma Formation) and phyllite (Ranimata Formation); no upper Nawakhot

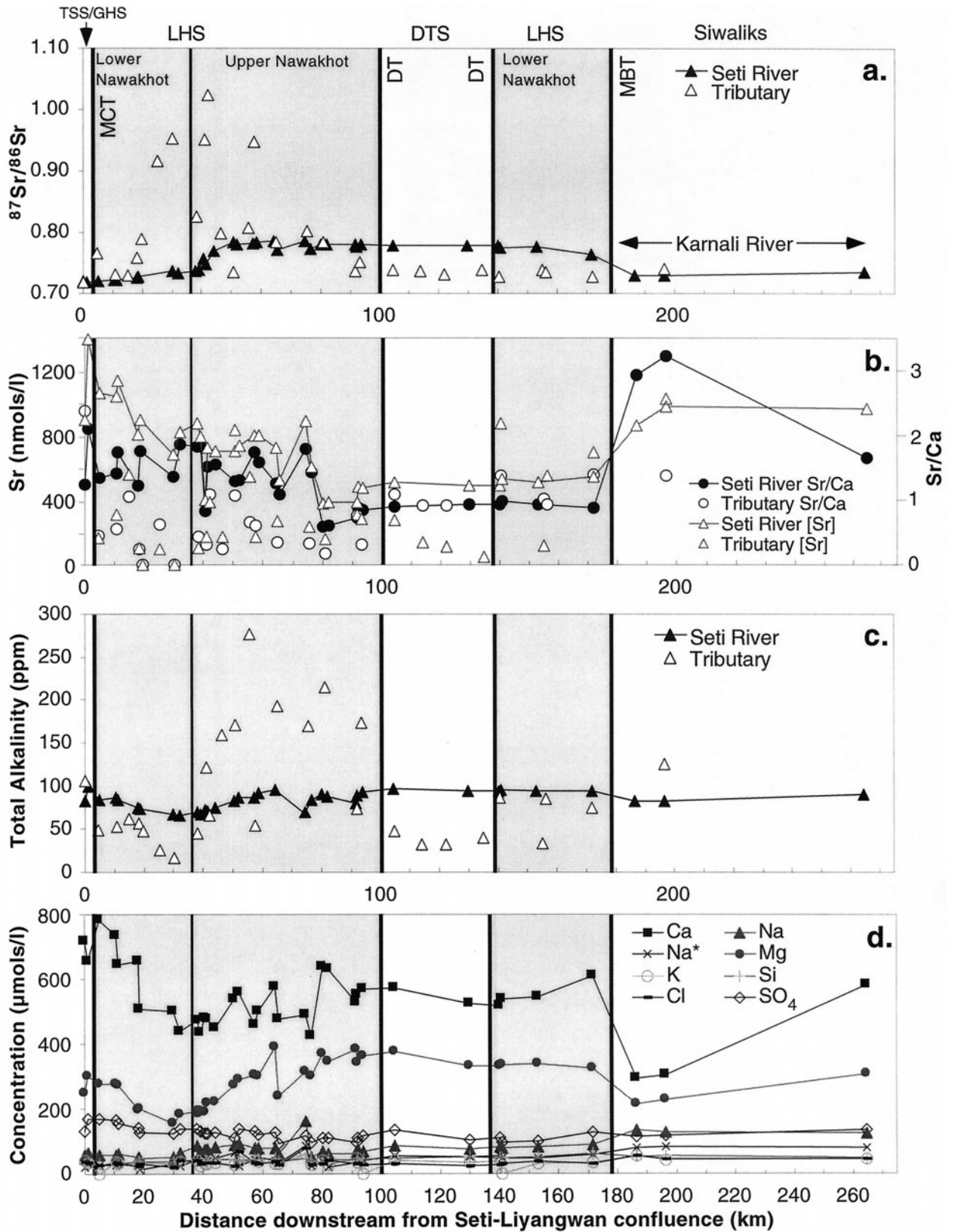


Fig. 2. Geochemical profiles of the Seti and tributary rivers (Table 3) downstream of the Seti-Liyangwan River confluence (Kilometer 0): (a)  $^{87}\text{Sr}/^{86}\text{Sr}$  ratios of the Seti River and tributaries. (b) Sr/Ca of the Seti River and concentration of Sr in the Seti River and tributaries. (c) Total alkalinity of the Seti River and tributaries. (d) Concentrations of major ions in the Seti River. The Seti River joins the Karnali at about Kilometer 180.

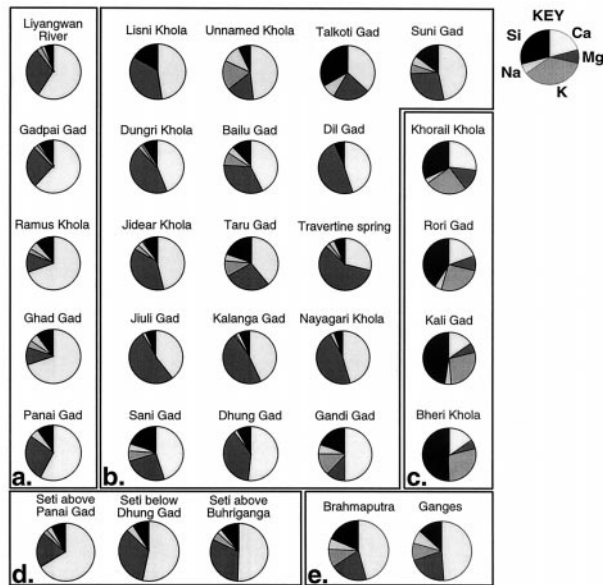


Fig. 3. Geochemical domains of Seti River tributaries (see text): (a) TSS/GHS domain. (b) LHS domain. (c) DTS domain. (d) Seti River. (e) Ganges and Brahmaputra Rivers. Diagrams represent molar proportions. Within boxes, uppermost tributaries are displayed from top to bottom and left to right.

dolostones are present. We did not sample any tributaries along this reach. Mainstem water chemistry remains constant, demonstrating that weathering of lower LHS silicates along this reach makes no contribution to the Seti. At this point, the Seti is joined by the Buhriganga, and ~18 km further downstream the Seti joins the Karnali River. These are large rivers that flow across multiple terranes, and their addition changes mainstem values greatly. This effectively puts an end to our detailed comparison of local geology with river chemistry. We report analyses of these larger rivers and all major tributaries in Tables 2 and 3.

#### 4.2. $\delta^{18}\text{O}$

$\delta^{18}\text{O}$  (VSMOW) values of the Seti River and tributaries correlate strongly ( $r^2 = 0.85$  using small tributaries) with watershed elevation (Table 3). This relationship will be used in the modeling portion of the paper as one means of estimating the addition of recharge in each terrane.  $\delta^{18}\text{O}$  values of tributaries are generally higher than the nearby Seti River. Large tributaries draining higher elevations (Kalanga Gad and Suni Gad) also have lower values than adjacent tributaries.

#### 4.3. Silicate and Carbonate Weathering

Our data from the Seti River are in agreement with other studies that show carbonates dominate weathering fluxes in Himalayan rivers (Harris et al., 1998; Singh et al. 1998; Galy et al., 1999). The importance of carbonate weathering in Seti tributaries is qualitatively apparent in the high correlation ( $r^2$ ) between  $(\text{Ca} + \text{Mg})$  and  $\text{HCO}_3^-$  of 0.97. Calcium versus  $\text{HCO}_3^-$  is less well-correlated at 0.78, indicating that both dolomite and calcite must be contributing to the carbonate weathering flux.

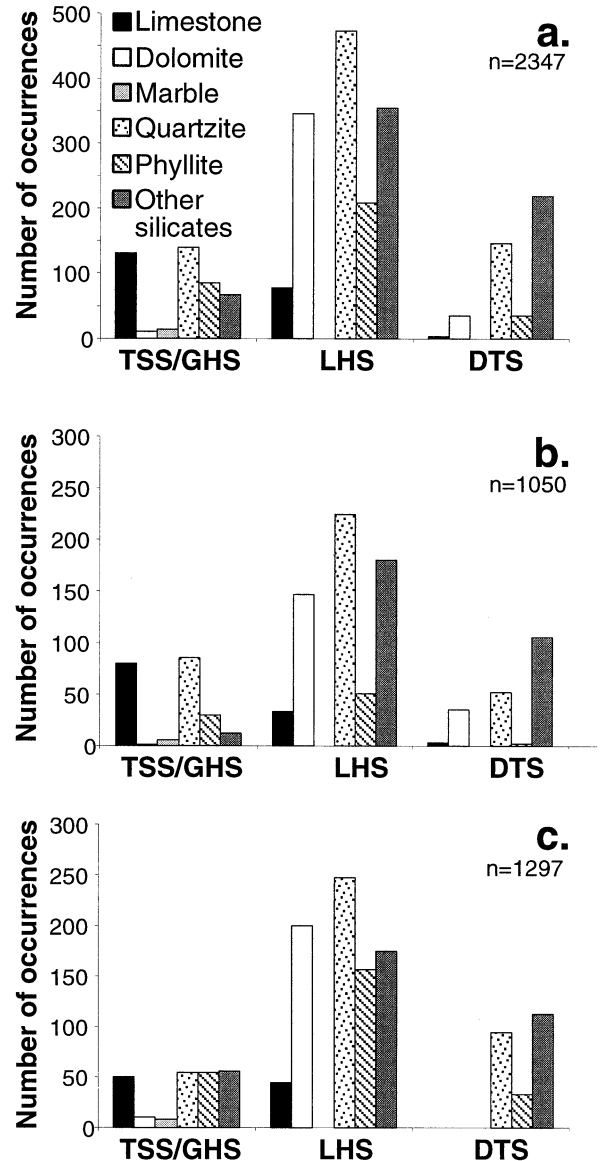


Fig. 4. Clast count histogram grouped by river domain: (a) Seti River and tributary clast counts combined. (b) Seti River clast counts. (c) Tributary clast counts. TSS/GHS-LHS boundary is below Panai Gad. LHS-DTS boundary is above Khorail Khola. Gandi Gad clasts are counted with LHS clasts.

There are several more quantitative methods used to evaluate silicate and carbonate weathering contributions to riverine TDS. Both methods account for atmospheric and evaporite input to TDS by subtracting 1 mol of Na for every mol of Cl present in the water (Jenkins et al., 1987; Singh et al., 1998). The corrected value ( $\text{Na}^*$ ) is used in all weathering budgets below, although the correction is generally minor.

The CaMg-weathering index quantifies the proportion of Ca and Mg in natural waters that arises from carbonate weathering (Harris et al., 1998). It is assumed that Ca and Mg are weathered from silicate minerals in an empirically derived proportion ( $\alpha$ ) to  $\text{Na}^*$ . With contributions to Ca and Mg from silicate weathering subtracted in this manner, the remaining Ca and Mg

Table 2.  $^{87}\text{Sr}/^{86}\text{Sr}$ , Sr, and Ca ratios for Seti and Tributary river carbonate detritus, pebbles, and bedrock.

Sample type and location	Mg/Ca	Sr/Ca <sup>a</sup>	% Carbonate	$^{87}\text{Sr}/^{86}\text{Sr}^b$	$^{87}\text{Sr}/^{86}\text{Sr}^c$	Sr/Ca <sup>a,c</sup>
Seti River carbonate detritus						
Seti above Liyangwan	0.03	26.31	27%	0.716785		23.41
Seti above Ramus Khola	0.08	8.55	25%	0.717617	0.717433	
Seti above Panai Gad	0.03	10.74	18%	0.716817		
Seti below Panai Gad	0.06	18.06	—	0.716944		
Seti above Talkoti Gad	0.09	14.63	24%	0.716106		
Seti above Suni Gad	0.10	12.45	25%	0.717821		
Seti above Jidear Khola	0.15	7.36	9%	0.718327	0.721527	7.24
Seti above Taru Gad	0.13	7.09	10%	0.721493		
Seti above Jiuli Gad	0.45	2.57	6%	0.738821	0.727908	2.32
Seti above Kalanga Gad	0.46	1.54	12%	0.727245		
Seti below Kalanga Gad	0.63	0.79	19%	0.740441		
Seti above Nayagari Khola	0.82	0.60	19%	0.736219	0.744074	0.97
Seti below Dhung Gad	0.52	0.99	7%	0.725054		
Seti below Dipayal	0.60	0.79	10%	0.752593		
Seti above Buhriganga	0.61	0.68	12%	0.734864		
Karnali at Chisapani	0.36	1.86	12%	0.723893		
Tributary River carbonate detritus						
Liyangwan River	0.07	9.98	30%	0.716902	0.717433	
Gadpai Gad	0.29	2.21	12%	0.745797		
Ramus Khola	0.08	5.99	10%	0.717853		
Ghad Gad	0.03	22.08	11%	0.715103		
Panai Gad	0.83	0.19	7%	0.795728		
Lisni Khola	0.86	0.29	17%	0.730269		
Dungri Khola	0.82	0.26	7%	0.812258	0.862562	0.25
Bailu Gad	0.89	0.74	3%	0.872169	1.012254	0.37
Dil Gad	0.90	0.31	18%	0.738230	0.748378	0.31
Jidear Khola	0.68	0.49	24%	0.741130		
Taru Gad	0.99	0.45	—	0.904907		
Jiuli Gad	0.84	0.29	20%	0.772956	0.771832	
Kalanga Gad	0.77	0.57	21%	0.746054	0.766705	
Nayagari Khola	0.59	0.20	38%	0.762711	0.750769	
Sani Gad	0.68	0.94	4%	0.722864		
Dhung Gad	0.61	0.21	53%	0.721483		
Gandi Gad	0.05	13.06	3%	0.725599		
Buhriganga	0.39	1.75	3%	0.799864		

<sup>a</sup> Sr/Ca ratios are in nmol/ $\mu\text{mol}$ .

<sup>b</sup> Uncrushed and unwashed sediments.

<sup>c</sup> Ratios of crushed and ammonium acetate washed sediments.

<sup>d</sup> All Sr/Ca and Mg/Ca ratios are molar ratios.

are assumed to derive from carbonate weathering. We use Kali Gad, a watershed underlain entirely by silicate rocks, to estimate  $\alpha$  (0.79) for this study. Using this approach, we find that carbonate weathering accounts for >95% of the TDS in the Seti River (Fig. 7a).

Another approach is the use of constitutive mass balance similar to the approach of Garrels and MacKenzie (1967) and as modified by Blum et al. (1998) for a watershed in the western Himalaya. Using this method we calculate a carbonate contribution to TDS of >70% in the Seti River (Fig. 7b,c).

Tributary waters display unique characteristics directly related to local geology. High TDS, high Sr, and high Ca/Mg-weathering indices in tributaries of the TSS/GHS are consistent with dominantly carbonate, especially limestone, weathering. Calcium accounts for >60% of the cations in solution, and  $\text{Ca}^{2+}$  and  $\text{HCO}_3^-$  are strongly correlated. Low Mg/Ca ratios in Tethyan limestones and in metamorphic marbles of the GHS detritus account for the similarly low ratios in river water (Tables 2 and 3).

The solute chemistry of tributaries draining the LHS is

strongly affected by the presence or absence of carbonate in the watershed. The tributaries draining silicates only, such as Un-named Khola and Talkoti Gad, are very dilute (<29 mg/L), have low Sr, and low Ca-Mg weathering indices. This is typical of rivers draining silicate rocks worldwide, and reflects the very slow weathering rates of LHS chlorites, muscovites, feldspars, and ferro-magnesian silicates compared to carbonates. All tributaries between Suni Gad and Dhung Gad drain some LHS carbonates. Dolostone is far more common in the LHS than in the TSS/GHS. These tributary waters all have high TDS and high Sr. Ca + Mg is strongly correlated with  $\text{HCO}_3^-$  in tributaries draining the upper Nawakhot Group ( $r^2 = 1.0$ ), and they have high Ca-Mg weathering indices and Mg/Ca ratios (Fig. 3), indicating a greater dolostone weathering contribution than in the TSS/GHS. Cation proportions in the Seti mainstem in this part of the LHS closely match average cation proportions in tributaries draining the upper Nawakhot Group (Fig. 3). The large Na spike above Kalanga Gad is probably related to the presence of a major stockyard at this point in the river, because K and Cl are also high and Mg/Na ratios are low.

Table 2 (cont.).  $^{87}\text{Sr}/^{86}\text{Sr}$ , Sr, and Ca ratios for Seti and Tributary river carbonate detritus, pebbles, and bedrock.

Sample type and location	Sample number	Rock type <sup>a</sup>	% Calcite	% Dolomite	Sr (ppm)	$^{87}\text{Sr}/^{86}\text{Sr}$	Sr/Ca <sup>b,c</sup>	Mg/Ca <sup>c</sup>	
<b>River Pebbles</b>									
Seti above Dhuli	44Arck	Mbl (GHS)	6%	1%	395	0.718034	0.07	0.22	
	44Brck	Ls (TSS)	40%	11%	346	0.722059	0.24	0.06	
	44Crck	Ls (TSS)	79%	6%	728	0.711330	3.09	0.11	
	44Drck	Ls (TSS)	21%	3%	486	0.751925	1.15	0.07	
	44Erck	Mbl (GHS)	11%	1%	230	0.713486	0.10	0.03	
	44Grck	Ls (TSS)	32%	1%	2548	0.724995	1.95	0.04	
	44Hrck	Ls (TSS)	48%	2%	612	0.715995	1.23	0.18	
	44Irck	Ls (TSS)	25%	6%	692	0.714740	0.27	0.06	
	Ramus Khola Ghad Gad	33Arck	Mbl (GHS)	19%	1%	1431	0.714025	1.11	0.09
		32Arck	Mbl (GHS)	37%	1%	793	0.714526	0.72	0.01
32Brck		Mbl (GHS)	48%	1%	936	0.715121	4.15	0.06	
32Crck		Mbl (GHS)	12%	1%	355	0.724044	0.07	0.02	
32Drck		Mbl (GHS)	71%	1%	1003	0.711147	1.45	0.01	
Seti below Talkoti Gad	32Erck	Mbl (GHS)	57%	1%	760	0.713750	2.56	0.05	
	34aArck	Ls (TSS)	28%	3%	486	0.737899	0.27	0.08	
	34aBrck	Ls (TSS)	60%	6%	1332	0.712795	1.53	0.07	
	34aCrck	Mbl (GHS)	63%	5%	367	0.713791	0.75	0.05	
	34aDrck	Mbl (GHS)	37%	2%	209	0.719609	0.22	0.11	
	34aErck	Ls (TSS)	39%	5%	1178	0.714980	1.09	0.04	
	34aFrck	Ls (TSS)	54%	3%	855	0.713954	1.38	0.20	
Seti below Taru Gad	7A no veins	DLs (LHS)	7%	14%	332	0.805204	0.67	0.86	
	7A vein	DLs (LHS)	55%	6%	499	0.829833	0.88	1.65	
	7Brck	Dolo (LHS)	0%	71%	90	0.716901	0.20	0.26	
	7Crck	DLs (LHS)	31%	11%	460	0.818455	0.48	1.52	
	7Drck	Dolo (LHS)	3%	77%	102	0.722584	0.20	1.60	
	7Erck	DLs (LHS)	1%	86%	44	0.715831	0.12	1.44	
	Seti above Buhriganga	65Arck	Dolo (LHS)	1%	89%	33	0.719046	0.04	0.33
65Brck		Dolo (LHS)	65%	30%	66	0.752391	0.18	1.59	
65Crck		Dolo (LHS)	1%	72%	69	0.710959	0.08	0.08	
Nayagari Khola	49arck	LDolo (LHS)	2%	47%	106	0.721794	0.12	1.68	
	49brck	Dolo (LHS)	0%	93%	37	0.820778	0.08	1.61	
	49Crck	DLs (LHS)	1%	93%	39	0.714813	0.08	1.62	
<b>Bedrock</b>									
Marble Boulder	41Arck	Mbl (GHS)	39%	2%	545	0.717065	0.70	0.05	
	41Brck	Mbl (GHS)	35%	2%	520	0.716983	3.53	0.14	
Phyllitic Marble	37Arck	Mbl (GHS)	35%	9%	1192	0.715639	1.20	0.14	
	37Brck	Mbl (GHS)	45%	8%	1112	0.715586	1.68	0.04	
	32Crck	Mbl (GHS)	12%	1%	355	0.724044	0.07	0.02	
Dolostone below Talkoti Gad	22Arck	Dolo (LHS)	5%	59%	70	0.756128	0.09	1.36	
	22Brck	Dolo (LHS)	10%	87%	61	0.770556	0.18	0.02	
Ulleri Gneiss	SR29	(DTS/LHS)	0%	5%	1248	1.026826	15.16	6.64	
Ranimata Phyllite (+qtz)	SR28	(LHS)	0%	7%	207	1.132635	0.30	1.49	
Ranimata Phyllite (+musc)	SR34	(LHS)	0%	4%	2199	0.915359	1.10	4.03	
Kushma Quartzite	SR19	(LHS)	0%	1%	311	0.870497	0.54	14.01	
Nayagari Khola Carbonate	45Arck	Dolo (LHS)	1%	52%	100	0.799053	0.24	1.74	
	45Brck	Dolo (LHS)	0%	48%	183	0.733430	0.12	1.59	
	45Crck	Dolo (LHS)	3%	147%	49	0.757555	0.31	1.55	
Chairo Khola Carbonate	71Arck	Ls (LHS)	67%	6%	69	0.767884	0.09	1.16	
	71Brck	Ls (LHS)	18%	78%	51	0.726730	0.10	1.69	
	71Crck	Ls (LHS)	0%	106%	33	0.707474	17.72	3.95	

<sup>a</sup> Rock type based on effervescence strength and texture: DLs = Dolomitic limestone; LDolo = Limey dolostone; Mbl = Marble (Source terrane).

<sup>b</sup> Sr/Ca ratios in nmol/ $\mu\text{mol}$ .

<sup>c</sup> All Sr/Ca and Mg/Ca ratios are molar ratio.

The solute chemistry of most tributaries draining the DTS is markedly different from most other tributaries studied. The low TDS, Sr, and Ca-Mg weathering indices all point to entirely silicate weathering, consistent with the total absence of carbonate in the bedload of these tributaries. Continued dissolution of carbonates in the Seti mainstem overwhelms any influence DTS tributaries may have on Seti River chemistry. The Seti

River maintains a geochemical composition most similar to the LHS Seti River and tributaries until it joins the Karnali River.

The solute chemistry of the Seti River also shares many essential features with that of larger Himalayan rivers. For example, major cation proportions in the Seti below the LHS are very similar to that of the Ganges/Brahmaputra (Fig. 3).

Table 3. Seti, Tributary, and Karnali River stream solute concentrations and isotopic values.

Sample name	Distance <sup>a</sup> (km)	Ca <sup>2+</sup> ( $\mu\text{mol/L}$ )	Mg <sup>2+</sup>	Na <sup>+</sup>	Na <sup>+</sup> <sup>b</sup> K <sup>+</sup>	Si	HCO <sub>3</sub> <sup>-</sup>	Cl <sup>-</sup>	SO <sub>4</sub> <sup>2-</sup>	Sr (nmol/L)	TDS (mg/L)	Mg/Ca	Sr/Ca <sup>c</sup>	<sup>87</sup> Sr/ <sup>86</sup> Sr	$\delta^{18}\text{O}$ (‰) VSMOW	
Seti River																
Seti above Liyangwan	0.00	531	222	82	42	44	69	1362	40	127	890	87	0.42	1.68	0.719469	-13.0
Seti below Liyangwan	1.25	656	299	64	30	34	70	1637	34	169	1381	105	0.46	2.10	0.718452	-12.9
Seti above Dhuli	5.00	646	273	111	55	45	67	1387	56	164	1056	98	0.42	1.63	0.720295	-12.4
Seti above Ramus Khola	10.60	581	255	127	93	38	65	1412	33	169	1037	95	0.44	1.78	0.721803	-12.4
Seti below Ramus Khola	11.25	611	260	67	-1	26	68	1375	68	161	1130	94	0.42	1.85	0.721989	-12.3
Seti above Panai Gad	18.05	556	190	122	95	36	82	1237	27	138	800	85	0.34	1.44	0.725459	-11.9
Seti below Panai Gad	18.75	506	200	47	15	35	78	1212	32	129	889	80	0.39	1.76	0.726655	-11.7
Seti above Talkoti Gad	30.00	499	153	53	32	31	85	1100	20	125	680	74	0.31	1.36	0.736024	-11.2
Seti below Talkoti Gad	32.25	439	183	67	25	37	82	1087	42	138	818	75	0.42	1.86	0.731852	-11.4
Seti above Suni Gad	38.00	474	194	87	45	42	91	1137	42	136	869	79	0.41	1.83	0.736748	-11.2
Seti below Suni Gad	39.25	434	192	70	39	26	83	1112	32	130	791	74	0.44	1.82	0.738387	-11.3
Seti above Dungri Khola	40.80	479	189	77	44	30	87	1187	34	123	396	78	0.39	0.83	0.755904	-11.1
Seti below Dungri Khola	41.50	477	216	77	43	30	81	1175	34	123	720	78	0.45	1.51	0.747443	-11.4
Seti below Bailu Gad	44.00	447	222	82	49	34	93	1225	33	126	696	79	0.50	1.56	0.769054	-11.4
Seti above Jidear Khola	50.60	539	272	89	64	28	93	1350	25	110	700	86	0.50	1.30	0.783622	-11.3
Seti below Jidear Khola	52.00	559	288	92	24	38	92	1425	68	136	734	94	0.52	1.31	0.779995	-11.1
Seti above Taru Gad	57.25	459	304	80	44	41	94	1425	36	132	795	89	0.66	1.73	0.781727	-10.9
(Duplicate)															0.781568	
Seti below Taru Gad	58.50	501	300	80	51	38	93	1500	29	122	795	91	0.60	1.59	0.783724	-11.2
Seti above Jiuli Gad	64.25	576	389	79	41	33	103	1574	38	128	721	99	0.67	1.25	0.785418	-10.7
Seti below Jiuli Gad	65.50	477	238	61	34	30	82	1200	27	94	522	76	0.50	1.09	0.770543	-10.9
Seti above Kalanga Gad	74.50	489	315	163	85	62	104	1137	78	119	881	85	0.64	1.80	0.785123	-10.8
Seti below Kalanga Gad	76.50	424	298	50	24	28	80	1375	27	98	604	80	0.70	1.42	0.773257	-10.4
Seti above Nayagari Khola	80.00	479	351	100	65	26	84	1487	34	116	378	90	0.73	0.79	0.779755	-8.7
Seti below Nayagari Khola	82.00	631	344	60	20	27	99	1437	40	109	386	94	0.54	0.61	0.779431	-10.2
Seti above Sani Gad	91.50	467	324	83	53	31	87	1312	30	104	386	83	0.69	0.83	0.780563	-10.1
Seti below Sani Gad	91.90	551	342	74	45	33	101	1462	30	111	483	92	0.62	0.88	0.776884	-9.8
Seti below Dhung Gad	93.75	569	361	69	42	—	96	1525	27	116	476	94	0.63	0.84	0.780841	-9.9
Seti above Khorail Khola	104.30	571	377	86	54	41	105	1587	32	134	508	100	0.66	0.89	0.777674	-9.7
Seti below Dipayal	129.75	524	331	77	53	34	108	1537	24	105	487	92	0.63	0.93	0.778829	-9.9
Seti above Gandhi Gad	140.00	519	332	84	55	40	104	1549	28	110	487	93	0.64	0.94	0.778743	-9.9
Seti below Gandhi Gad	140.90	539	336	80	49	—	107	1562	31	97	527	92	0.62	0.98	0.775343	-10.0
Seti above Buhriganga	153.00	546	339	84	48	30	113	1549	36	101	507	94	0.62	0.93	0.775627	-9.8
Seti above Chaira Khola	171.80	609	323	90	58	35	132	1537	32	129	539	99	0.53	0.88	0.763348	-9.6
Tributary Rivers																
Liyangwan River	0.00	734	375	73	42	13	70	1737	30	228	1746	118	0.51	2.38	0.717852	-12.9
Gadpai Gad	4.50	369	149	23	23	—	55	800	—	116	164	56	0.40	0.45	0.765128	-10.4
Ramus Khola	10.75	444	87	91	65	54	85	862	27	107	310	64	0.20	0.70	0.730596	-10.5
Ghad Gad	15.00	536	84	50	32	34	82	1012	19	98	560	69	0.16	1.04	0.728293	-11.1
Panai Gad	18.25	329	193	85	60	35	71	937	25	45	102	57	0.59	0.31	0.758555	-10.2
Lisni Khola	19.75	252	185	74	54	32	72	787	19	29	—	47	0.73	—	0.789141	-9.7
Unnamed Khola	25.25	156	55	75	58	35	23	431	17	38	96	29	0.35	0.61	0.916815	-9.1
Talkoti Gad	30.25	92	55	41	20	—	84	281	21	23	—	20	0.60	—	0.953543	-8.4
Suni Gad	38.25	237	137	50	24	28	79	737	26	56	101	46	0.58	0.43	0.825201	-10.8
Dungri Khola	41.00	546	539	47	28	27	105	1999	19	41	170	105	0.99	0.31	0.950671	-9.7
(Duplicate)															0.951298	
Bailu Gad	42.25	359	278	90	62	42	98	1087	28	95	390	70	0.77	1.09	1.022884	-10.5
(Duplicate)															1.022900	
Dil Gad	46.50	696	765	24	-2	—	95	2599	26	100	172	138	1.10	0.25	0.798606	-9.5
Jidear Khola	50.75	781	634	70	49	63	156	2799	21	158	835	155	0.81	1.07	0.734700	-9.3
(Duplicate)															0.734660	
Travertine spring	55.75	841	1707	134	75	95	203	4536	59	422	550	266	2.03	0.65	0.807528	
(Duplicate)															0.808214	
Taru Gad	57.50	292	208	71	71	30	143	900	—	60	176	56	0.71	0.60	0.946555	-10.0
Jiuli Gad	65.00	773	1029	42	10	27	118	3149	32	274	267	183	1.33	0.35	0.783687	-8.8
Kalanga Gad	75.50	714	782	52	20	39	99	2787	32	141	235	151	1.10	0.33	0.802487	-9.7
Nayagari Khola	81.00	928	955	38	0	39	118	3511	38	62	157	179	1.03	0.17	0.783503	-7.7
Sani Gad	91.75	412	232	99	60	41	172	1212	39	73	309	76	0.56	0.75	0.736353	-8.1
Dhung Gad	93.25	906	683	67	29	0	152	2849	38	44	282	150	0.75	0.31	0.750843	-7.8
Khorail Khola	104.50	252	125	285	234	30	304	787	51	118	275	66	0.49	1.09	0.738614	-6.8

(Continued)

Table 3. (Continued)

Sample name	Distance <sup>a</sup> (km)	Ca <sup>2+</sup> ( $\mu\text{mol/L}$ )	Mg <sup>2+</sup>	Na <sup>+</sup>	Na <sup>+</sup> + <sup>b</sup> K <sup>+</sup>	Si	HCO <sub>3</sub> <sup>-</sup>	Cl <sup>-</sup> SO <sub>4</sub> <sup>2-</sup>	Sr (nmol/L)	TDS (mg/L)	Mg/Ca	Sr/Ca <sup>c</sup>	<sup>87</sup> Sr/ <sup>86</sup> Sr	$\delta^{18}\text{O}$ (‰) VSMOW		
Spring at Dadeldurah													0.729602			
Rori Gad	113.88	152	68	237	204	28	315	525	33	74	138	47	0.45	0.91	0.737108	-7.4
Kali Gad	122.00	123	49	243	217	34	377	525	26	39	111	44	0.40	0.91	0.731563	-7.7
Unai Gad	134.75	—	—	—	—	—	—	662	—	—	46	20	—	—	0.738930	-7.7
Gandi Gad	140.50	639	144	243	179	74	240	1412	65	176	878	106	0.23	1.37	0.727224	-7.7
Bheri Khola	155.00	116	40	241	209	0	356	550	32	23	118	41	0.35	1.01	0.737937	-7.2
Buhriganga	156.25	604	200	91	64	50	143	1400	27	121	557	92	0.33	0.92	0.734227	-8.8
Chairo Khola	172.00	497	148	151	114	32	194	1225	37	80	696	79	0.30	1.40	0.727415	-6.8
Thuli Gad	196.38	751	352	251	219	46	207	2062	31	152	1031	130	0.47	1.37	0.740063	-7.1
Karnali River																
Karnali below the Seti	186.38	534	249	196	141	54	108	1350	54	115	855	91	0.47	1.60	0.729569	
Karnali above Thuli Gad	196.38	584	254	168	123	35	120	1362	45	117	975	92	0.44	1.67	0.729675	
Karnali at Chisapani	264.63	581	308	123	79	47	102	1487	44	133	959	97	0.53	1.65	0.734993	-10.7

<sup>a</sup> Distance downstream from Seti–Liyangwan confluence.

<sup>b</sup> Na-Cl.

<sup>c</sup> Sr/Ca is in nmol/ $\mu\text{mol}$ .

One reason is that the Seti drains the same basic suite of terranes as other large rivers tributary to the Ganges. Another reason is that the Seti as well as the larger Himalayan rivers carry abundant carbonate detritus derived from the LHS and TSS. Thus, continued weathering of highly soluble carbonate buffers the major element chemistry of these rivers along their entire lengths.

#### 4.4. Sr Budget

There are several methods for determining the relative weathering contribution of silicates versus carbonates to the Sr budget of rivers. One common approach is to compare Sr/Ca ratios of bedrock and associated waters, assuming the congruent dissolution of Sr, Ca, Na, and Cl during weathering, and to calculate the proportion of riverine Sr from silicate and carbonate weathering. Singh et al. (1998) used this approach in the Indian Himalaya and Galy et al. (1999) in Himalayan watersheds to the east of our study area. The latter derived the following equations:

$$[Sr]_{Ev} = [Cl]_{Riv}^* \times \left( \frac{[Sr]}{[Cl]} \right)_{Ev} \quad (1)$$

$$[Sr]_{Sil} = ([Na]_{Riv}^* - [Cl]_{Riv}^*) \times \left( \frac{[Sr]}{[Na]} \right)_{Sil} \quad (2)$$

$$[Sr]_{Carb} = ([Ca]_{Riv}^* - 0.2 \times ([Na]_{Riv}^* - [Cl]_{Riv}^*)) \times \left( \frac{[Sr]}{[Ca]} \right)_{Carb} \quad (3)$$

where  $Sr_{Ev}$ ,  $Sr_{Sil}$ , and  $Sr_{Carb}$  represent the Sr flux from evaporites, silicates, and carbonates, respectively. Strontium–ion ratios in parentheses are average bedrock ratios (Table 4). Applying this in the Narayani watershed of central Nepal, Galy et al. (1999) found that silicates contribute >50%, carbonates < 40%, and evaporites < 10% of the total Sr. Using Eqns. (3) and (4), we found that 85% and 37–95% (mean = 69%) of the Sr in the Seti mainstem draining TSS and LHS terranes, respectively, is derived from carbonate weathering. These esti-

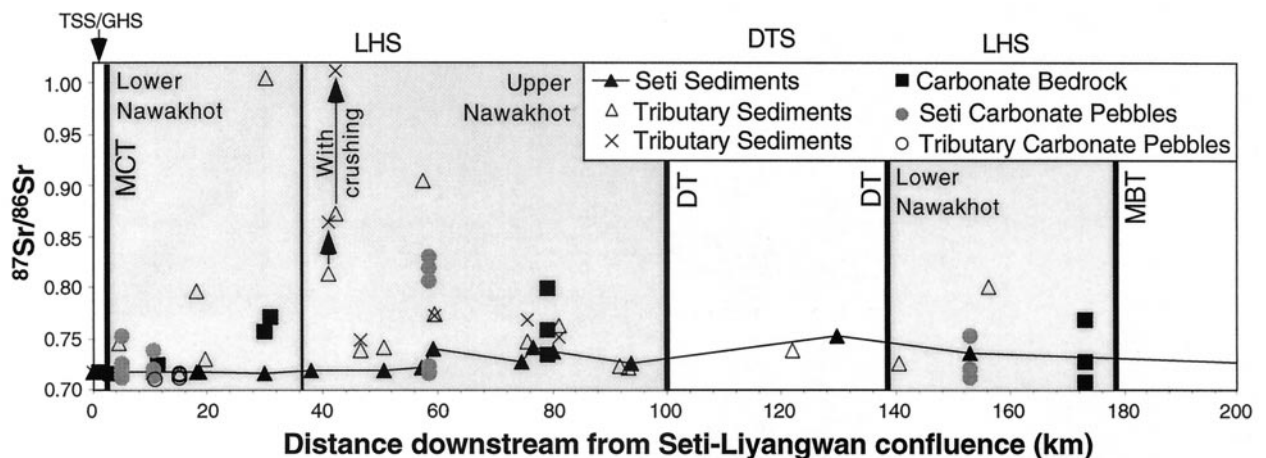


Fig. 5. <sup>87</sup>Sr/<sup>86</sup>Sr profile of Seti River and tributary carbonate sediments, pebbles, and bedrock (Table 2).

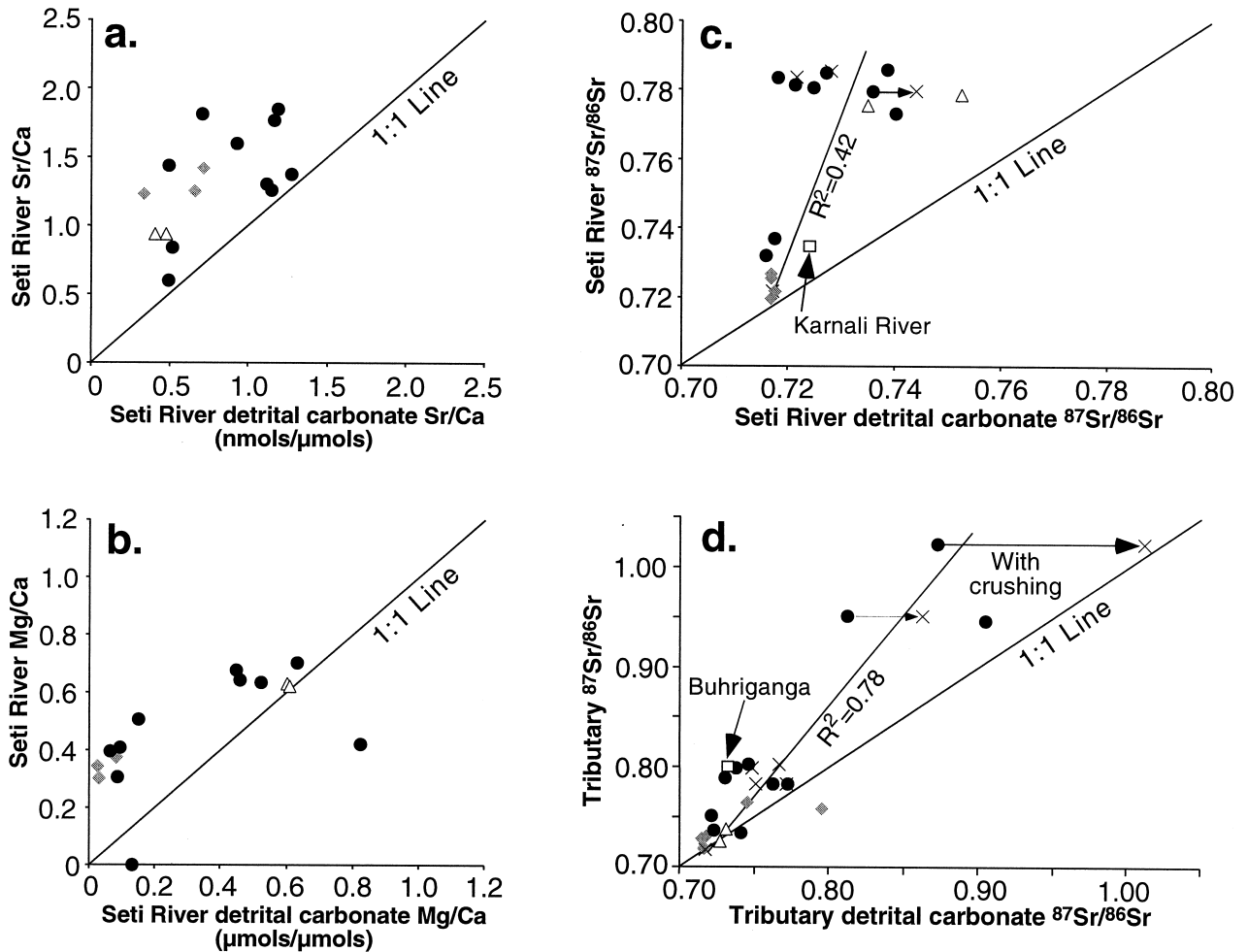


Fig. 6. Ionic ratios of the Seti River waters and associated carbonate detritus: (a) Seti River Sr/Ca. (b) Seti River Mg/Ca. (c) Seti River  $^{87}\text{Sr}/^{86}\text{Sr}$ . (d) Tributary  $^{87}\text{Sr}/^{86}\text{Sr}$ . Diamonds = TSS/GHS rivers; circles = LHS rivers; triangles = DTS rivers; squares = other rivers. X = crushed sediment values correlated with uncrushed sample on same horizontal level.

mates are close to those (80% for TSS; 40–50% for LHS) of Galy et al. (1999) for the Kali Gandaki watershed.

The key assumptions of this approach are that the Sr/Ca (or Sr/Na) ratio of bedrock is released congruently to river waters during weathering, that the range of values for carbonate and silicate rocks do not overlap significantly, and that the ratios of the end-members are well characterized. If either incongruent dissolution takes place or the Sr/Ca ratios of silicate and carbonate bedrock have a wide range of significantly overlapping values (Table 2), then this approach is problematic. In the Himalayas, Galy et al. (1999) assume a Sr/Ca ratio (mmol/mol) of 1 for carbonates and congruent dissolution; any ratio in excess of this in Himalayan waters is taken to indicate weathering of silicates because silicates generally have higher Sr/Ca ratios than carbonates.

In aquatic systems dominated by carbonate rocks, numerous studies show that Sr and Ca are not congruently released during carbonate dissolution (McKinley and Oliver, 1991; Banner, 1995; Thomas et al., 1991; Bishop et al., 1994). In general, Ca is favored over Sr in the calcite lattice (Lorens, 1981). In natural systems, the  $K_D^{\text{Sr-Ca}}$  of calcite ranges from 0.02 to 0.09

(Banner, 1995), thereby increasing the ratio of Sr/Ca in groundwaters compared to the Sr/Ca ratio of the dissolving carbonate. This partitioning can occur through partial dissolution of detrital carbonate, which could be occurring because detrital carbonate persists in bedloads of Himalayan rivers all the way to the sea (Quade et al., 1997); or partitioning may occur as secondary carbonate forms. Seti waters are all near or exceed calcite saturation, and secondary calcite forms along the length of the hydrologic system. Thick secondary travertine is very common in bedrock fractures, particularly in the Lakharpata Formation, and in spring seeps above the Seti River. Downstream, pedogenic carbonate and sandstone cements are ubiquitous in basin-fill deposits such as the Siwalik Group. The partitioning of Sr and Ca during calcite formation on the modern Ganges River is visible in elevated Sr/Ca ratios of Gangetic river and groundwater (Palmer and Edmond, 1992). These studies would suggest that Sr/Ca ratios in Himalayan rivers may be elevated by incongruent dissolution and reprecipitation of calcite, and not by silicate weathering. As pointed out by Galy et al. (1999), this effect will produce overestimates of the silicate contribution to Sr in Himalayan rivers.

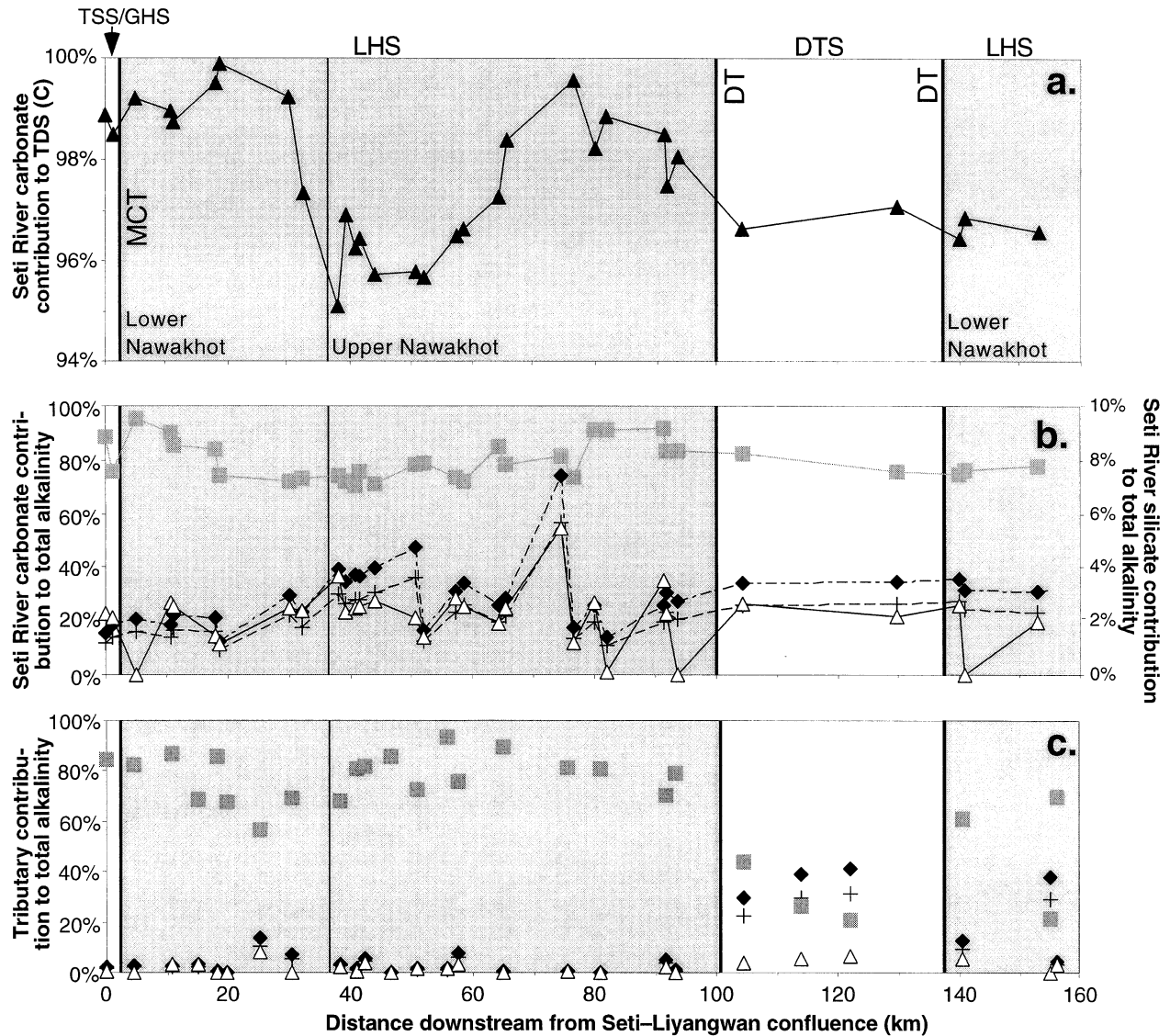


Fig. 7. Indexes of carbonate weathering in the Seti River: (a) Percent carbonate contribution to weathering using the CaMg-weathering index of Harris et al. (1998). Percent contribution to weathering in (b) the Seti River and (c) Seti tributaries using the mass balance calculations of Blum et al. (1998). For (b) and (c): squares are contribution to total alkalinity from carbonates; diamonds are from albite to kaolinite; crosses are from anorthite to kaolinite; and triangles are from biotite to vermiculite. Accounting for the input of Na from precipitation and percent total alkalinity attributed to orthoclase to kaolinite weathering have been omitted for clarity.

Several lines of evidence suggest to us that the contribution to dissolved mainstem Sr from carbonates is higher than 50%. First, the largest increases in  $^{87}\text{Sr}/^{86}\text{Sr}$  ratios and Sr values coincide with reaches of the river where carbonates occur. In reaches where little or no carbonate is present,  $^{87}\text{Sr}/^{86}\text{Sr}$  ratios in the mainstem show little or no change, and Sr decreases. Second, in the mainstem reach flowing through carbonate-rich LHS below Suni Gad,  $1/\text{Mg}$  versus  $^{87}\text{Sr}/^{86}\text{Sr}$  ratios is well-correlated (Fig. 8). There is no such correlation between  $1/\text{Sr}$  or  $1/\text{Na}$  and  $^{87}\text{Sr}/^{86}\text{Sr}$  ratio (Figs. 8, 9). These patterns point to a two-endmember system controlled by limestone (low  $^{87}\text{Sr}/^{86}\text{Sr}$  and low Mg) in the TSS/LHS, and by more radiogenic dolostone (high  $^{87}\text{Sr}/^{86}\text{Sr}$  and high Mg) in the LHS. Alternatively, the high Mg endmember represents a Mg-rich silicate such as

Table 4. Summary of Sr concentrations and ranges of  $^{87}\text{Sr}/^{86}\text{Sr}$  ratios.

Rock type	Sr concentration (ppm)	$^{87}\text{Sr}/^{86}\text{Sr}$
Sialic silicates (Global)	No published data	$>0.710\text{--}1.0^a$
Carbonates (Global)	500–2000 <sup>a,b</sup>	0.706–0.709 <sup>a</sup>
TSS Carbonates	150 <sup>c</sup> –2500 <sup>b</sup>	0.720–0.733 <sup>c</sup>
GHS Silicates	80–300 <sup>d</sup>	0.75–1.0 <sup>e</sup>
GHS Marbles <sup>h</sup>	60–1200 <sup>b</sup>	0.71–0.77 <sup>f,h</sup>
LHS Carbonates	500 <sup>e</sup>	0.722–0.734 <sup>e</sup>
LHS Dolomites	30–300 <sup>g,h</sup>	0.706–0.8935 <sup>g,h</sup>
LHS Vein calcite <sup>h</sup>	500 <sup>h</sup>	0.820–0.829 <sup>f,h</sup>

Sources are: <sup>a</sup> Palmer and Edmond, 1992; <sup>b</sup> Bishop et al., 1994; <sup>c</sup> Harris et al., 1998; <sup>d</sup> Gardner and Walsh, 1996; <sup>e</sup> Krishnaswami et al., 1992, Singh et al., 1998; <sup>f</sup> Blum et al., 1998; <sup>g</sup> Quade et al., 1997; <sup>h</sup> denotes value from this study.

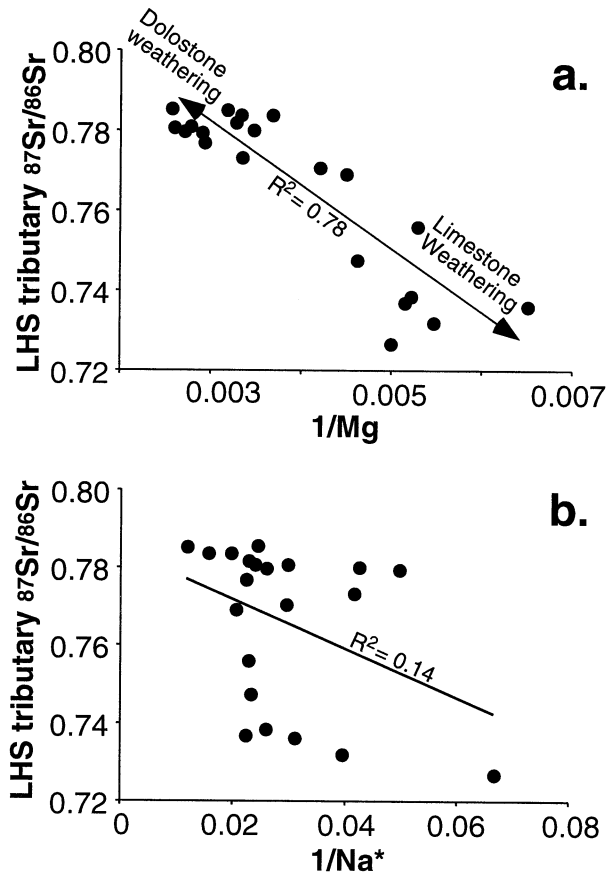


Fig. 8.  $^{87}\text{Sr}/^{86}\text{Sr}$  plotted against (a)  $1/\text{Mg}$  and (b)  $1/\text{Na}^*$  for Seti River waters in the LHS.

chlorite, which occurs widely in the LHS but is especially common in the Ranimata Formation. The problem with this alternative is that the Ranimata Formation is extensively exposed far upriver of the major increase in  $^{87}\text{Sr}/^{86}\text{Sr}$  and Mg values in the Seti mainstem below Suni Gad. What is geologically unique about the Suni Gad watershed is the first appearance in clast counts of abundant dolostones of the Lakharpata Formation.

#### 4.5. Sr Budget Modeling

We can model the relative fluxes of Sr originating from the TSS/GHS, LHS, and DTS into the modern Seti River. Using these models and our understanding of the structural development of the region, we can also estimate the relative contributions of each terrane to Sr flux and the  $^{87}\text{Sr}/^{86}\text{Sr}$  ratios of the Seti River at 15 and 25 Ma. Estimates of absolute fluxes cannot be made without discharge data which are currently unavailable for this watershed. We use two approaches to calculate the average  $^{87}\text{Sr}/^{86}\text{Sr}$  ratio, Sr concentrations and relative discharges of Seti River watersheds. The first approach utilizes mixing relationships of  $\delta^{18}\text{O}$  values in tributary and mainstem waters, and the second uses tributary area as a proxy for discharge (Table 5).

#### 4.6. Model Set-up

##### 4.6.1. $\delta^{18}\text{O}$ -based model

We use a simple oxygen isotope mass balance model to calculate the amount of water entering the Seti River from each tributary. This model assumes that all changes in the  $\delta^{18}\text{O}$  of the mainstem are due to the addition of tributary water, ignoring groundwater input, evaporation, and rainfall directly onto the river. Where we did not sample the Seti River above or below a tributary, the tributary  $^{87}\text{Sr}/^{86}\text{Sr}$  and Sr concentration is geometrically averaged with either the upstream or downstream tributary, respectively. The averaged  $^{87}\text{Sr}/^{86}\text{Sr}$  and Sr concentration of both tributaries is then treated as a single tributary in the flux model. When combined with relative contributions of water from the  $\delta^{18}\text{O}$  measurements, this yields a Sr flux for each tributary:

$$F_{\text{TSS/GHS}} = \sum Q_{\text{tributary}} \times [\text{Sr}]_{\text{tributary}} \quad (4)$$

$$R_{\text{endriner}} = \frac{F_{\text{TSS/GHS}}}{F_{\text{total}}} \times R_{\text{TSS/GHS}} + \frac{F_{\text{LHS}}}{F_{\text{total}}} \times R_{\text{LHS}} + \frac{F_{\text{DTS}}}{F_{\text{total}}} \times R_{\text{DTS}} \quad (5)$$

where  $Q$  is the relative discharge specific to each terrane (we use the TSS/GHS as an example),  $F$  is Sr flux, and  $[\text{Sr}]$  and  $R$  are the average Sr concentration and  $^{87}\text{Sr}/^{86}\text{Sr}$  ratio of the river, respectively.  $R_{\text{endriner}}$  and  $[\text{Sr}]_{\text{endriner}}$  are the modeled  $^{87}\text{Sr}/^{86}\text{Sr}$  ratio and Sr concentration of the Seti River below Gandi Gad, respectively.

##### 4.6.2. Tributary area based (TAB) model

In this model, we assume that tributary area is proportional to tributary discharge and  $^{87}\text{Sr}/^{86}\text{Sr}$  ratios and Sr concentrations of tributaries are weighted by area, as follows:

$$Q_{\text{TSS/GHS}} = \sum P_{\text{tributary}} \times A_{\text{tributary}} \quad (6)$$

$$R_{\text{TSS/GHS}} = \sum \left( \frac{A_{\text{tributary}}}{A_{\text{TSS/GHS}}} \times R_{\text{tributary}} \right) \quad (7)$$

$$[\text{Sr}]_{\text{TSS/GHS}} = \sum \left( \frac{A_{\text{tributary}}}{A_{\text{TSS/GHS}}} \times [\text{Sr}]_{\text{tributary}} \right) \quad (8)$$

where  $P$  is precipitation and  $A$  is area. Precipitation estimates are based on regional meteorologic data presented previously. We add unsampled drainage areas (Fig. 1) to the next measured downstream tributary's area and assume a similar  $^{87}\text{Sr}/^{86}\text{Sr}$  ratio. The  $R_{\text{endriner}}$  and  $[\text{Sr}]_{\text{endriner}}$  values are then calculated using Eqns. (6–8).

##### 4.6.3. Model results

Both the  $\delta^{18}\text{O}$  and TAB models accurately predict the Sr concentrations and  $^{87}\text{Sr}/^{86}\text{Sr}$  ratios of the modern-day Seti River (Table 5). Using modern precipitation estimates (Masek et al., 1994), the  $\delta^{18}\text{O}$  model matches Sr within 4% and  $^{87}\text{Sr}/^{86}\text{Sr}$  ratios within 1% of the actual values (500 nmol/L and 0.7753). Both models are most sensitive to changes in Sr concentrations, with a 0.0116 change in the  $R_{\text{endriner}}$  for a 100 nmol/L change in the average LHS Sr concentration. In the TSS/GHS, a 0.01 change in average  $^{87}\text{Sr}/^{86}\text{Sr}$ , a 0.1 m/yr

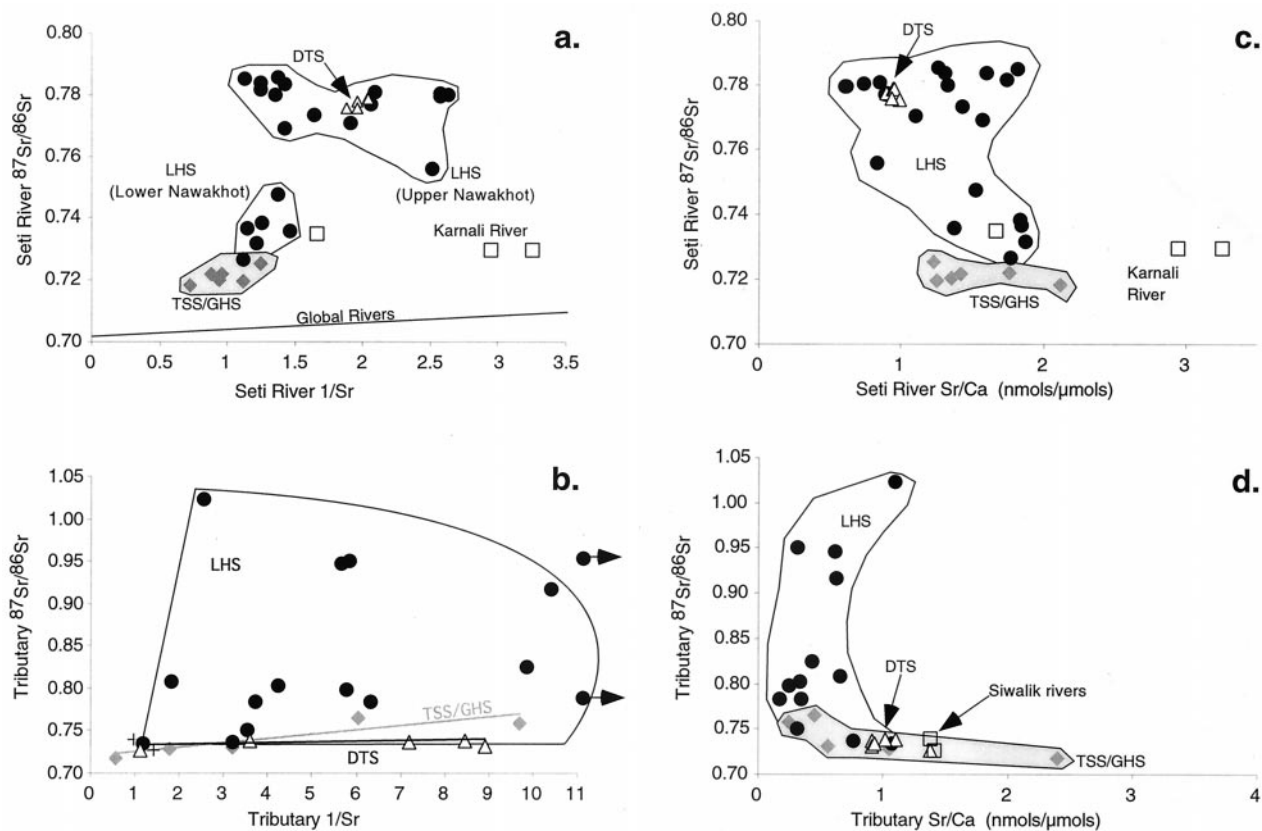


Fig. 9. Scatter diagrams of  $^{87}\text{Sr}/^{86}\text{Sr}$  vs.  $\text{Sr}/\text{Ca}$  and  $1/\text{Sr}$ . (a) and (c) are filtered Seti River waters; (b) and (d) are filtered tributary waters. Global river line from Palmer and Edmond (1992). Symbols are the same as in Fig. 6.

change in precipitation, or a 100 nmol/L change in the Sr concentration changes the  $R_{\text{endriver}}$  by 0.0022 (excluding changes in LHS Sr concentration). Changes in the DTS have less of an effect than changes in the LHS or TSS/GHS. Using the  $\delta^{18}\text{O}$  model for the present, the LHS contributes 53% of the total modeled Sr flux, the TSS/GHS 39%, and the DTS 8%.

For the 15 and 25 Ma models, we use the Sr concentrations and  $^{87}\text{Sr}/^{86}\text{Sr}$  ratio of 100 nmol/L and 0.713 for TSS rivers and the Sr concentrations and  $^{87}\text{Sr}/^{86}\text{Sr}$  ratios from Ramus Khola as proxies for GHS rivers. We use evidence from DeCelles et al. (1998a,b) to estimate the aerial extent of the TSS/GHS, LHS, and DTS for models at 15 Ma and 25 Ma. Precipitation estimates are based on plant fossil evidence in the Siwaliks that the Himalayas were no drier than today (Awashi and Prasad, 1989). We do not attempt to quantify seasonal differences in dissolved flux. Although the total flux of TDS is greater during the monsoon (Galy and France-Lanord, 1999), we assume the proportions of TDS remain constant and do not affect our results.

Sr fluxes at 15 and 25 Ma are most affected in our model by the contribution from the TSS and LHS terranes. At 15 Ma, the TSS contributes 89% of the total Sr flux to the Ganges River system. The TSS contributes approximately 98% of the total dissolved Sr entering the Ganges from the Seti River at 25 Ma. This is in agreement with other studies that suggest the TSS dominates dissolved Sr fluxes (Galy et al., 1999) to the Ganges prior to exposure of the LHS. However, Galy et al. (1999)

attribute high  $^{87}\text{Sr}/^{86}\text{Sr}$  ratios and low Sr fluxes in Himalayan rivers during the last 10 Ma to decreased carbonate Sr fluxes and a climatically driven increase in silicate weathering. We attribute high  $^{87}\text{Sr}/^{86}\text{Sr}$  ratios and low Sr fluxes during the last 10 Ma to: 1) increased Sr fluxes from newly exposed LHS dolostones with high  $^{87}\text{Sr}/^{86}\text{Sr}$  and low Sr; and 2) decreased Sr fluxes from TSS rocks, with low  $^{87}\text{Sr}/^{86}\text{Sr}$  and high Sr, in the Himalayan rain-shadow.

#### 4.7. Implications for the Marine $^{87}\text{Sr}/^{86}\text{Sr}$ record and Cenozoic $\text{CO}_2$

Much of the large increase in the marine  $^{87}\text{Sr}/^{86}\text{Sr}$  record over the past 40 Ma is widely viewed as a result of silicate weathering in the Himalaya, a process that consumes  $\text{CO}_2$  and may therefore have gradually cooled Cenozoic climate. Our findings, that carbonate weathering controls the Sr budget of Himalayan rivers and can be highly radiogenic, suggest that changes in the  $^{87}\text{Sr}/^{86}\text{Sr}$  ratio in the ancestral Ganges–Brahmaputra are independent of silicate weathering rates in the Himalaya, and therefore independent of atmospheric  $\text{CO}_2$  or climate change. Likewise, changes in the marine  $^{87}\text{Sr}/^{86}\text{Sr}$  record may also prove independent of silicate weathering rates.

## 5. CONCLUSIONS

Our study shows that geology exerts strong controls on the solute chemistry of the Seti River and its tributaries. In agree-

Table 5. Seti River Sr flux model.

<b>Modern Seti River (Area based model)</b>					
	Q Relative	[Sr] $\mu\text{mol/L}^a$	$^{87}\text{Sr}/^{86}\text{Sr}^e$	Flux	Contribution to total Sr flux <sup>d</sup>
TSS/GHS-MCT	1226	1.04	0.7234	1273	36%
LHS	5583	0.25	0.8278	1411	40%
DTS	2562	0.31	0.7353	806	23%
SIW			0.7200		
				Total flux (dimensionless) = 3490	
	Rainfall (m)	Area (km)	$^{87}\text{Sr}/^{86}\text{Sr}$ at Seti below Gandi Gad 0.768 Sr concentration at Seti below Gandi Gad 554 nmol/L		
TSS/GHS-MCT	1	1226			
LHS	2.2	2538			
DTS	2	1281			
SIW	2 n				
<b>Modern Seti River (<math>\delta^{18}\text{O}</math> based model)</b>					
	Q Relative <sup>g</sup>	[Sr] $\mu\text{mol/L}^b$	$^{87}\text{Sr}/^{86}\text{Sr}^f$	Flux	Contribution to total Sr flux <sup>d</sup>
TSS/GHS-MCT	1245	0.92	0.7252	1139	39%
LHS	7159	0.22	0.8071	1557	53%
DTS	968	0.26	0.7317	251	9%
SIW			0.7200	0	0%
				Total flux (dimensionless) = 2948	
	Rainfall (m)	$\delta^{18}\text{O}$ Contribution <sup>c</sup>	$^{87}\text{Sr}/^{86}\text{Sr}$ at Seti below Gandi Gad 0.769 Sr concentration at Seti below Gandi Gad 491 nmol/L		
TSS/GHS-MCT	1	13%			
LHS	2.2	76%			
DTS	2	10%			
SIW	2				
<b>15 Ma Seti River (Area based model)</b>					
	Q Relative	[Sr] $\mu\text{mol/L}^a$	$^{87}\text{Sr}/^{86}\text{Sr}^d$	Flux (f)	Contribution to total Sr flux <sup>d</sup>
TSS	1500	1	0.713	1500	51%
GHS	2250	0.3	0.730	675	23%
TSS	750	1	0.713	750	26%
				Total flux (dimensionless) = 2925	
	Rainfall (m)	Area (km)	$^{87}\text{Sr}/^{86}\text{Sr}$ at Seti below Gandi Gad 0.717 Sr concentration at Seti below Gandi Gad 838 nmol/L		
TSS	0.5	3000			
GHS	1.5	1500			
TSS	1.5	500			
<b>25 Ma Seti River (Area based model)</b>					
	Q Relative	[Sr] $\mu\text{mol/L}^a$	$^{87}\text{Sr}/^{86}\text{Sr}^d$	Flux (f)	Contribution to total Sr flux <sup>d</sup>
TSS	2400	1	0.713	2400	58%
GHS	750	0.3	0.730	225	5%
TSS	1500	1	0.713	1500	36%
				Total flux (dimensionless) = 4125	
	Rainfall (m)	Area (km)	$^{87}\text{Sr}/^{86}\text{Sr}$ at Seti below Gandi Gad 0.714 Sr concentration at Seti below Gandi Gad 962 nmol/L		
TSS	0.8	3000			
GHS	1.5	500			
TSS	1.5	1000			

<sup>a</sup> Sr concentrations are weighted to relative watershed area.

<sup>b</sup> Sr concentrations weighted to relative  $\delta^{18}\text{O}$  contribution.

<sup>c</sup> Relative contributions to Q calculated from  $\delta^{18}\text{O}$  data.

<sup>d</sup> Percentages are rounded and may not sum to 100%.

<sup>e</sup>  $^{87}\text{Sr}/^{86}\text{Sr}$  ratios are weighted to relative watershed area.

<sup>f</sup>  $^{87}\text{Sr}/^{86}\text{Sr}$  ratios are weighted to relative  $\delta^{18}\text{O}$  contribution.

<sup>g</sup> Normalized to area based Q relative.

ment with other studies (Harris et al., 1998; Galy et al., 1999), weathering budgets show that >70% of the TDS in the Seti River is derived from carbonate weathering. Seti River Sr is derived mainly from the weathering of carbonate rocks in the TSS/GHS and upper Nawakhot Group of the LHS. Silicate

rocks in the TSS/GHS, LHS (lower Nawakhot Group) and DTS have little influence on Seti River  $^{87}\text{Sr}/^{86}\text{Sr}$  ratios. Sr budgets that use the bedrock Sr/Ca ratios of carbonates to determine Sr fluxes probably underestimate the contribution of carbonate weathering to the Sr flux. Incongruent carbonate dissolution or

reprecipitation of calcite from water strongly favors Sr in solution and elevates Sr/Ca ratios of natural waters above carbonate bedrock ratios.

Our modeling indicates that weathering of TSS/GHS and LHS rocks contributes the most Sr to the modern-day Seti River. In the past, riverine  $^{87}\text{Sr}/^{86}\text{Sr}$  was buffered by carbonate rocks of the TSS with high Sr but low  $^{87}\text{Sr}/^{86}\text{Sr}$  ratios. Modeled  $^{87}\text{Sr}/^{86}\text{Sr}$  ratios remained low ( $\sim 0.715$ ) until the unroofing of metacarbonate rocks in the LHS after  $\sim 15$  Ma. Over time, the contribution of the TSS to river Sr has probably been reduced by the development of the Himalayan rainshadow.

Our results suggest that the rise in  $^{87}\text{Sr}/^{86}\text{Sr}$  ratios in the Cenozoic marine record is not produced by increased silicate weathering rates in the Himalaya (Raymo and Ruddiman, 1992; Singh et al., 1998; Edmond, 1992; Krishnaswami et al., 1992). Instead, we find that weathering of dolomite and limestone dominates the Sr budget of the Seti. The abundance of carbonate in all major Himalayan rivers, and the general similarity of cation chemistry between the Seti and Ganges/Brahmaputra indicate to us that carbonate weathering dominates the Sr flux in all these systems. If correct, the use of the marine  $^{87}\text{Sr}/^{86}\text{Sr}$  record to infer rates of silicate weathering in the Himalaya is unwarranted.

*Acknowledgments*—We wish to thank B. N. Upreti, T. P. Ojha, B. LaReau, P. Kaminski, and D. Robinson for their adventurous assistance in the field and J. Patchett, C. E. Isachsen, and G. E. Gehrels for their patient assistance in the lab. This paper has greatly benefited from informal discussions with J. L. Drever, J. L. Banner, and J. Blum. We also wish to thank two anonymous reviewers for their comments. This work was supported by NSF grant #EAR 97-25607.

## REFERENCES

- Asahara Y., Tanaka T., Kamioka H., and Nishimura A. (1995) Asian continental nature of  $^{87}\text{Sr}/^{86}\text{Sr}$  ratios in north central Pacific sediments. *Earth Planet. Sci. Lett.* **133**, 105–116.
- Washii N. and Prasad M. (1989) Siwalik plant fossils from Surai Khola area, western Nepal. *Paleobotanist* **38**, 298–318.
- Banner J. L. (1995) Application of the trace element and isotope geochemistry of strontium to studies of carbonate diagenesis. *Sedimentology* **42**, 805–824.
- Berner E. K. and Berner R. A. (1987) *The Global Water Cycle*. Prentice-Hall.
- Bishop P. K., Smalley P. C., Emery D., and Dickson J. A. D. (1994) Strontium isotopes as indicators of the dissolving phase in a carbonate aquifer: Implications for the  $^{14}\text{C}$  dating of groundwater. *J. Hydrology* **154**, 301–321.
- Blum J. D., Gazis C. A., Jacobson A. D., and Chamberlain C. P. (1998) Carbonate versus silicate weathering in the Raikhot watershed within the High Himalayan crystalline series. *Geology* **26**, 411–414.
- Burg J. P. and Chen G. M. (1984) Tectonics and structural zonation of southern Tibet. *Nature* **311**, 219–223.
- Central Bureau of Statistics (1998) *Statistical Pocket Book, Nepal*. His Majesty's Government National Planning Commission Secretariat. Kathmandu, Nepal.
- DeCelles P. G., Gehrels G. E., Quade J., Ojha T. P., Kapp P. A., and Upreti B. N. (1998a) Neogene foreland basin deposits, erosional unroofing, and the kinematic history of the Himalayan fold-thrust belt, western Nepal. *Bull. Geol. Soc. Am.* **110**, 2–21.
- DeCelles P. G., Gehrels G. E., Quade J., and Ojha T. P. (1998b) Eocene–early Miocene foreland basin development and the history of Himalayan thrusting, western central Nepal. *Tectonics* **17**, 741–765.
- DePaolo D. J. and Ingram B. L. (1985) High-resolution stratigraphy with strontium isotopes. *Science* **227**, 938–941.
- Edmond J. M. (1992) Himalayan tectonics, weathering processes, and the strontium isotope record in marine limestones. *Science* **258**, 1594–1597.
- Galy A., France-Lanord C., and Derry L. A. (1999) The strontium isotopic budget of Himalayan rivers in Nepal and Bangladesh. *Geochim. Cosmochim. Acta* **63**, 1905–1925.
- Galy A. and France-Lanord C. (1999) Weathering processes in the Ganges–Brahmaputra basin and the riverine alkalinity budget. *Chem. Geol.* **159**, 31–60.
- Gardner R. and Walsh N. (1996) Chemical weathering of metamorphic rocks from low elevations in the Southern Himalaya. *Chem. Geol.* **127**, 161–176.
- Garrels R. M. and MacKenzie F. T. (1967) in *Equilibrium Concepts in Natural Water Systems* (ed. R. G. Gould) *Amer. Chem. Soc. Adv. Chem. Ser.* **67**, 222–242.
- Harris N., Bickle M., Chapman H., Fairchild I., and Bunbury J. (1998) The significance of Himalayan rivers for silicate weathering rates: Evidence from the Bhote Kosi tributary. *Chem. Geol.* **144**, 205–220.
- Hodges K. V., Parrish R. R., and Searle M. P. (1996) Tectonic evolution of the central Annapurna Range, Nepalese Himalayas. *Tectonics* **15**, 1264–1291.
- Jenkins M. D., Drever J. I., Reider R. G., and Buchanan T. (1987) Chemical composition of fresh snow on Mount Everest. *J. Geophys. Res.* **92**, 10,999–11,002.
- Krishnaswami S., Trivedi J. R., Sarin M. M., Ramesh R., and Sharma K. K. (1992) Strontium isotopes and rubidium in the Ganga–Brahmaputra river system: Weathering in the Himalaya, fluxes to the Bay of Bengal and contributions to the evolution of oceanic  $^{87}\text{Sr}/^{86}\text{Sr}$ . *Earth Planet. Sci. Lett.* **109**, 243–253.
- Lorens R. B. (1981) Sr, Cd, and Co distribution coefficients in calcite as a function of calcite precipitation rate. *Geochim. Cosmochim. Acta* **45**, 553–561.
- Macfarlane A. M. (1993) Chronology of tectonic events in the crystalline core of the Himalaya, Langtang National Park, central Nepal. *Tectonics* **12**, 1004–1025.
- Masek J. G., Isacks B. L., Gubbels T. L., and Fielding E. J. (1994) Erosion and tectonics at the margins of continental plateaus. *J. Geophys. Res.* **99**, 13,941–13,956.
- McKinley P. W. and Oliver T. A. (1991) Meteorological, stream-discharge, and water-quality data for 1986–1991 from two small basins in central Nevada. *Open-File Report* 93-0651.
- Molnar P., England P., and Martinod J. (1993) Mantle dynamics, uplift of the Tibetan Plateau, and the Indian monsoon. *Rev. Geophys.* **31**, 357–396.
- Montañez I. P., Banner J. L., Osleger D. A., Borg L. E., and Bosserman P. J. (1996) Integrated Sr isotope variations and sea-level history of Middle to Upper Cambrian platform carbonates: Implications for the evolution of Cambrian seawater  $^{87}\text{Sr}/^{86}\text{Sr}$ . *Geology* **24**, 917–920.
- Palmer M. R. and Edmond J. M. (1992) Controls over the strontium isotope composition of river water. *Geochim. Cosmochim. Acta* **56**, 2099–2111.
- Pearson P. N. and Palmer M. R. (1999) Middle Eocene seawater pH and atmospheric carbon dioxide concentrations. *Science* **284**, 1824–1826.
- Quade J., Chivas A. R., and McCulloch M. T. (1995) Strontium and carbon isotope tracers and the origins of soil carbonate in South Australia and Victoria. *Palaeo. Palaeo. Palaeo.* **113**, 103–117.
- Quade J., Roe L., DeCelles P. G., and Ojha T. P. (1997) The late Neogene  $^{87}\text{Sr}/^{86}\text{Sr}$  record of lowland Himalayan rivers. *Science* **276**, 1828–1831.
- Raymo M. E. and Ruddiman W. F. (1992) Tectonic forcing of late Cenozoic climate. *Nature* **359**, 117–122.
- Raymo M. E. and Ruddiman W. F. (1988) Influence of late Cenozoic mountain building on ocean geochemical cycles. *Geology* **16**, 649–653.
- Searle M. P. (1986) Structural evolution and sequence of thrusting in the High Himalayan, Tibetan Tethys and Indus suture zones of Zaskar and Ladakh, western Himalaya. *J. Struct. Geol.* **8**, 923–926.
- Singh S. K., Trivedi J. R., Pande K., Ramesh R., and Krishnaswami S. (1998) Chemical and strontium, oxygen, and carbon isotopic compositions of carbonates from the source waters of the Ganga, Ghagara, and Indus rivers. *Geochim. Cosmochim. Acta* **62**, 743–755.
- Thomas J. M., Lyles B. F., and Carpenter L. A. (1991) Chemical and isotopic data for water from wells, springs, and streams in carbonate-rock terrane of southern and eastern Nevada and southeastern California, 1985–1988. *USGS Open-File Report*, 1991. 89-0422.